9. CFD Modeling of Fluid Flow in CRDM Nozzle and Weld Cracks and through Annulus

In this section, we describe the results of the detailed computational fluid dynamics (CFD) modeling effort that we undertook to develop a better understanding and definition of the thermal hydraulic conditions in the CRDM nozzle annulus and developing wastage cavity at both CRDM Nozzles 2 and 3.

These thermal hydraulic conditions included fluid velocities, temperatures, pressures and steam quality (wetness), as well as the local temperature of the alloy steel RPV head material and CRDM nozzles in the annulus and wastage cavity as the leakage flow rate gradually increased and the cavity grew.

The CFD modeling work that we have completed has provided considerable insights into these critical thermal hydraulic parameters at various crack sizes, leak rates, cavity sizes, and relative axial positions of the wastage cavity and crack. In turn, these insights have allowed us to relate the predicted thermal hydraulic conditions from the model to potential metal removal rates by mechanical jet cutting, molten metaboric acid corrosion, flow assisted corrosion, and possibly concentrated aqueous boric acid corrosion/erosion.

Section 9.1 provides a brief overview of the FENOC root cause report conclusions regarding some of the key thermal hydraulic conditions and potential conditions, which provided a starting point for our modeling work. Section 9.2 summarizes the various possible metal removal mechanisms that can occur depending on the fluid and cavity thermal hydraulic conditions.

Section 9.3 describes our overall approach to the CFD modeling, and a brief description of the CFD model itself. Section 9.4 presents the results of our analysis of nozzle and weld crack leak flow rate as a function of crack length, which was a necessary input to the CFD model.

Sections 9.5, 9.6 and 9.7 summarize some of the key thermal hydraulic conditions predicted by the model such as velocity magnitude and direction, temperature, pressure, steam quality and oxygen content of the flowing fluid, as well as the low alloy steel

cavity wall temperature, for a number of cases that we consider relevant to the development and growth of the wastage cavities at Nozzles 2 and 3.

These results predicted by the CFD model cover conditions in the nozzle annulus, the wastage cavity and the space above the RPV head. Section 9.5 summarizes the RPV head wastage rates for various temperature, velocity, and fluid flow conditions.

9.1 Prior Assessments of Thermal Hydraulic Environments in the CRDM Annulus and Developing Wastage Cavity

Subsequent to the discovery of the large wastage cavity at Davis-Besse CRDM Nozzle 3, FENOC instituted a root cause investigation to analyze and document the inspection findings and operational history, review industry experience with CRDM nozzle cracking and boric acid corrosion, and develop a root cause explanation for the wastage.

The report generated by the FENOC root cause investigation team represents an exceptional effort to evaluate, analyze and synthesize a very large body of relevant industry and plant specific data and information in a relatively short time frame.[1]

The FENOC root cause investigation team concluded that "leakage from PWSCC cracks was "a necessary precursor to the material loss adjacent to nozzles 2 and 3, and that "these leaks led to local environmental conditions that produced modest material loss around nozzle 2 and much more extensive degradation around nozzle 3", and went on to note that:[2]

> "Given the current limited experimental data applicable to the observed degradation and the lack of existing detailed analytical calculations of the thermal-hydraulic and thermo-chemical environment along the nozzle leak path, it is not possible to definitely state the exact progression of mechanisms that led to the observed material loss.
>
> The environment along the leak path - from the primary system pressure inside the CRDM nozzle, through the axial PWSCC crack extending above the top of the J-groove weld, up through the annulus or cavity on the periphery of the

nozzle, and then out to the ambient pressure above the top head surface - is the result of complex processes such as critical two-phase flow, two-phase frictional and acceleration pressure drops, boiling heat transfer, boiling point elevation due to boric acid solution concentration, oxygen and hydrogen transport, various electrochemical processes, convective heat transfer on the surfaces of the head, and conduction heat transfer within the head materials.

Therefore, a detailed description of the damage progression including the precise physical mechanisms with a quantitative breakdown of the relative importance of each mechanism would be speculative."

Despite this lack of knowledge, the root cause team felt that the degradation modes at the two extremes of the overall progression could be defined: [3]

The first extreme is associated with the lack of material loss and extremely small leak rates observed for most of the leaking CRDM nozzles in the industry. For these extremely low leakage rates (on the order of 10^{-6}, 10^{-5} gpm) the leaking flow completely vaporizes to steam immediately downstream of the principal flashing location, most likely at the exit of the PWSCC crack. The result is to keep the gap between the nozzle and head dry, precluding high rates of low alloy steel material loss. In addition, the small velocities associated with the extremely small leakage preclude the flow mechanisms from being active."

"The other extreme of the degradation progression is associated with the large cavity located adjacent to nozzle 3. For this cavity, it is clear that the degradation proceeded by the classic boric acid corrosion mechanism associated with liquid boric acid solution concentrated through boiling and oxygen directly available for corrosion from the ambient atmosphere. The magnitude of the boiling heat transfer associated with the relatively high leak rate of nozzle 3 is sufficient to cool the head enough to allow liquid solution to cover the walls of the cavity."

With these two bounds, the root cause team went on to identify and provide qualitative descriptions of the possible mechanisms that may have been responsible for RPV head material loss, from the initial leakage and cavity formation to the final observed state of

the large cavity at CRDM Nozzle 3, and from these descriptions develop a "viable progression of events".[4]

The root cause report goes on to provide a qualitative description that the root cause investigation team had developed of the sequence of four "stages" that were thought to be involved in the development of the initial wastage cavity Davis-Besse nozzle 3 and its progression to the final state discovered in 2002. Briefly these were:[5]

- **Stage 1 - Crack initiation and progression to through wall**: The PWSCC crack at Nozzle 3 initiated in 1990 (+/- 3 years), and grew to through wall at a rate consistent with industry data to above the weld in the 1994 to 1996 time period. The initial leak rate from this crack would have been miniscule and not detectable.

- **Stage 2 - Minor Weepage/Latency Period:** Leakage into the annular region between the Alloy 600 nozzle and the low alloy steel base material of the RPV head. While the annulus is tight, single-phase erosion is possible, and several forms of boric acid corrosion are also possible that would open the annular gap. The relatively low crack growth rates compared with potential metal removal rates from the annulus would ensure that the crack dimensions continued to dominate the flow resistance since the annular space would be continually growing as metal removal takes place. The majority of the pressure drop remains across the crack and not the annulus, approximately 45% of the leak flow flashes upon discharge, and heat transfer from the metal surfaces rapidly vaporizes the rest. Thus, boric acid is both atomized with the steam and deposited as molten boric acid on the surrounding surfaces, with moisture escaping as steam.

- **Stage 3:** Deep annulus corrosive attack. As the annulus grows faster than the crack growth and leak flow, the annulus velocity decreases. Single phase erosion would decrease, and forms of flow accelerated corrosion, droplet impingement, and flashing induced corrosion could

become dominant. Deep annulus corrosive attack begins as the crack grows and the leak flow increases to the point where localized cooling of the RPV head steel occurs, resulting in more aggressive corrosion from a concentrated, aerated boric acid solution. It is probable that a small amount of material would be preferentially corroded in the vicinity of the crack, and the corrosion rate can be substantially greater in areas of greater velocity due to the potential for oxygen ingress into the annulus.

- **Stage 4 - General Boric Acid Corrosion:** As the crack grows and the leak rate through the crack increases, heat transfer from the surrounding metal is no longer sufficient to immediately vaporize the portion of leakage that does not flash and a substantial localized cooling effect of the RPV head steel in the cavity occurs. The result is that the annulus begins to overflow or expel liquid, causing an area to be wetted underneath the accumulations of boric acid on the RPV head. General boric acid corrosion on the wet, oxygenated surface of the low-alloy steel RPV head progresses rapidly. As general corrosion progresses, it would tend to carve out a "bowl" of corroded (or, oxidized) material which would fill with a saturated boric acid solution. High corrosion rates are possible due to the presence of concentrated aerated boric acid, and the bowl would both deepen and widen. When the liquid at the corrosion front reaches the depth of the stainless steel, downward progression ends. Throughout the majority of this process, being predominantly top-down, the annulus could remain somewhat intact until the approaching general corrosion front overcomes it, because the lower part of the annular region just above the crack would remain somewhat protected by the upward flow of deoxygenated water and steam. Thus, flashing effluent from the crack would be directed upward and out of the annulus while the annulus is in place. However, as soon as the low alloy steel corrosion front is below the elevation of the crack, the crack flow would be

directed laterally. This would undoubtedly change the degree of atomization of boric acid and affect the particle size of the boric acid carryover late in the process. The point at which the corrosion depth reached the crack location might have been around May 2001. At that time, the cleaning frequency of containment air coolers (CACs) due to boric acid fouling decreased.

The root cause report also concluded that the corrosion rate began to increase significantly starting at about 11RFO (1998) and acted for a four-year period of time. This implied an average corrosion rate of about 2.0 inches/year, and a maximum corrosion rate near the end of Cycle 13 of about 4.0 inches/year.[6] The report further noted that "further effort is ongoing to better define the corrosion rates based on the final measured size of the cavity and thermal-hydraulic modeling being performed by the MRP."

As we discussed earlier in Section 6.4.1, the EPRI MRP effort essentially adopted this probable sequence of stages, and a similar description is provided in the MRP "Statement of Work" for RPV head boric acid corrosion testing. This descriptive document outlines the work that the MRP intended to pursue in an effort to develop an understanding of the various corrosion mechanisms that were thought to be involved, and for which experimental data was lacking.

We have summarized the considerable discussion in the FENOC root cause report on this issue because it was, and to our knowledge remains, the most complete description of the possible sequence of events that lead to the formation of the large cavity at CRDM Nozzle 3. It provided us with a starting point to develop further understandings of the rate of crack growth, leakage increase, and metal removal processes.

However, it was clear that in order to develop a more complete and accurate explanation and a more definitive sequence of events timeline, we would need to at least begin to tackle the major task identified by the root cause team. This was the development of a more quantitative understanding of the thermal hydraulic conditions in the annular crevice and the wastage cavity over time, in order to better assess the potential for

different metal removal processes and rates to exist at different times. We undertook the CFD modeling work with this objective in mind.

We should note here that we have been fortunate in that we have had the benefit of information that the FENOC root cause team did not have. The CFD modeling work which has allowed us to define the thermal hydraulic conditions in the annulus and wastage cavity is the more obvious of these, and the root cause team had already identified this as vital information. However, there are other important bodies of information that we have benefited from that the FENOC root cause team did not available. The most important of these are:

- The results of the detailed metallurgical examinations of the nozzle remains, weld region, and large wastage cavity from CRDM Nozzle 3. This not only provided invaluable information on the nozzle, weld, and cavity, it identified the large weld crack at Nozzle 3. This weld crack was in line with the wastage cavity, had not been found during the NDE inspection prior to the nozzle removal, and clearly contributed significantly to leakage and cavity growth once it uncovered late in the sequence of events.

- The work recently published by the NRC/ANL (November 2006) provides definitive information on the crack growth rates (CGRs) specifically for CRDM nozzle Alloy 600 material (see Section 8.3.2). This new data established that the CGRs for the Nozzle 3 material were much higher than had been previously thought, being at the 95th percentile of the industry data and up to four times faster than the CGR's for Alloy 600 generally used by the industry, and on which the FENOC root cause team in part based its timeline of events.

- The boric acid corrosion data recently published by both the EPRI MRP in July 2006 (see section 6.4.1) and more importantly by the NRC/ANL in July 2005 (see Section 6.4.2) for thermal hydraulic conditions that were thought to be present in the annular crevice and

wastage cavity at various times during the evolution and growth of leakage of the wastage cavity at Davis-Besse CRDM Nozzle 3.[a] The NRC test program in particular provided reliable and quantitative data to show that molten metaboric acid at high temperatures above the melting point, if re-wetted by moisture, can result in high corrosion rates of low alloy steel comparable to those obtained in concentrated, aerated, aqueous boric acid.

The impact of some this new information has already been discussed in prior sections of this report, and we will integrate both it and the results we have derived from the CFD modeling work in the following sections of this report.

9.2 RPV Head Low Alloy Steel Removal Mechanisms and Wastage Rates

The following mechanisms for metal removal have been identified as potentially being involved at different times in the wastage process at CRDM Nozzles 2 and 3. These cover the entire range from purely mechanical metal removal processes, to corrosion processes in boric acid solutions under different flowing, immersion and impingement conditions.

Mechanical Metal Removal: Metal removal at very high rates can occur if the fluid velocity is high enough. Fluid velocities of up to 2,400 fps are required for water jet cutting or steam jet cutting (see Appendix E). However, leaking CRDM flanges were shown to readily steam cut due to boric acid leakage.

Abrasive Water Jet Cutting: This could occur with boric acid or steel particles if the velocity is high enough, and more moderate velocities (300fps to 1,000fps) are needed than for pure steam and/or water. There must be entrained particles in the fluid stream

[a] It is indicative of the value of the FENOC root cause team efforts to define a possible sequence of events that both EPRIMRP and the NRC/ANL test programs were guided by the qualitative description of the process developed by the root cause team in defining appropriate conditions for the corrosion test programs they undertook.

such as boric acid crystals, iron corrosion products, metal cuttings removed by water jet cutting, etc. to achieve maximum metal removal rates (see Appendix E).

Jet Impingement Metal Removal: Test programs both before and after the 2002 Davis-Besse event have shown that high velocity nozzle jets of high-temperature, high-pressure simulated reactor coolant impinging on an alloy steel corrosion specimen can cause erosion/corrosion rates from 4 to 11 inches/year depending on the distance from the jet orifice. Penetration rates were found to be higher at lower flow rates, but volumetric metal removal rates were higher with higher flow (Sections 6.3.1, 6.4.1).

Flow Assisted Corrosion (FAC): Flow assisted corrosion (FAC) can occur if the environment is corrosive and the velocities are on the order of 30 fps. FAC can result in up to an order of magnitude increase in metal removal rate.

Re-wetted Molten Metaboric Acid: A recent test program conducted by the NRC and ANL found that corrosion rates of up to 6 inches per year can occur from re-wetted molten metaboric acid (Section 6.4.2). Molten metaboric acid is formed by evaporation of water from aqueous boric acid solution and subsequent heating above both the phase transition temperature of 336°F and the melting point of 457°F. Moisture/wetness is necessary since the molten metaboric acid phase itself is non-corrosive to steel if dry conditions present. The deposits on the Davis-Besse RPV head caused no corrosion until they were wetted by the large leak flow in the last few months of operation prior to March 2002.

Aerated/Unaerated Concentrated Boric Acid: Corrosion by aerated/un-aerated concentrated boric acid at low temperatures in the 200-230°F range can result in corrosion rates of up to 7 to 8 inches per year if concentrated aqueous boric acid can be maintained in the wastage cavity (see Sections 6.3, 6.4.1, 6.4.2)

The thermal-hydraulic modeling results that we report in this section suggest that high velocities could have significantly accelerated wastage cavity growth on the RPV head by purely mechanical metal removal processes and/or FAC. The evidence that these "flow enhanced" material removal mechanism played a major role in the formation of the wastage cavity is shown in Figure 9.24 and 9.25 (see also Figures 10.2, 10.3). These

figures show the section of RPV head containing the wastage cavity that was removed for analysis.

The significant conclusion that can be reached by studying this image is the fact that boric acid corrosion alone did not form this cavity. If only concentrated aqueous boric acid corrosion was causing the wastage cavity growth, the cavity would have formed on a line that was directly toward the "down hill" direction due to the effects of gravity. Since the cavity is slightly angled to the right in this figure and since the CRDM nozzle and weld cracks that leaked to form this cavity were situated at approximately 10 degrees, it is obvious that the accelerated flow resulting from the leaking nozzle and weld cracks dramatically influenced the formation of the wastage cavity.

The extremely high maximum velocities (over 2,000 fps) noted near the crack exit in some of the CFD model runs indicate other material removal mechanisms were likely to have been operable at critical times in these regions. The momentum of the water droplets traveling at these velocities is sufficient to initiate material removal (see Appendix E). With the addition of abrasive particles (such as iron oxide corrosion products or boric acid crystals) to the flowing liquid droplets, significant material removal rates as high as (10 mm^3/s = 2.2 in^3/hour) can be achieved. Under ideal abrasive jet cutting conditions, these material removal rates could form the wastage cavity in as little as one or two weeks.

9.3 Approach to CFD Modeling and Model Development

9.3.1 Overall Approach to CFD Modeling

The CFD modeling builds on the results of Section 8 of this report, where we first performed a detailed stress analysis of the nozzle and weld region for CRDM nozzles 2 and 3. Using the results of that stress analysis, we then developed a more precise definition of the growth rates for the axial cracks at CRDM Nozzle 3 (nozzle and weld) and at Nozzle 2 (nozzle) than had previously been possible. This is because our analysis of crack growth rates (CGRs) used the recently published results of an experimental program conducted by ANL for the NRC, which has made available experimental measurements of CGRs for specific Alloy 600 material samples taken from Davis-Besse

CRDM Nozzle 3, as well as Alloy 182 samples from the Davis-Besse CRDM Nozzle 11 J-groove weld (see Section 8.3.2).

Starting with the known crack lengths and crack profiles for the various axial nozzle cracks in CRDM Nozzles 2 and 3 (as defined by the UT examination in February 2002) and with the CGRs described above, we were able then to develop a realistic timeline for the growth of cracks both through the Alloy 182 weld and in the Alloy 600 nozzle itself.

An independent analysis of leak rate as a function of crack size and morphology then gave us a reasonable estimate of the leak rates from the various nozzle cracks. The detailed metallurgical examination of the remains of Nozzle 3 and its associated J-groove weld provided invaluable information regarding the morphology of the large axial weld crack in the center of the large wastage cavity at Nozzle 3, from which we were also to generate a reasonable estimate of the leak flow rate through the weld crack once it was uncovered by the wastage cavity.

All of this provided information that allowed the definition of appropriate boundary and input conditions for a number of CFD case studies of crack size, leak rate, and wastage cavity size that were designed to generate the detailed thermal hydraulic conditions relevant to the development of the wastage cavity over time. The output from these case studies, which we describe in detail in Sections 9.5 and 9.6, allowed us to assess the possible metal removal mechanisms – mechanical, flow assisted corrosion (FAC), molten boric acid and aqueous boric acid corrosion - that were more likely than not to have been involved or controlling at various stages in the overall development and growth of the wastage cavity.

9.3.2 CFD Model Development

A computational fluid dynamics (CFD) model of the wastage cavity that formed on the RPV head of the Davis-Besse nuclear reactor due to CRDM leaks was constructed to determine the varying thermal hydraulic fluid conditions that developed in the annulus and cavity around CRDM Nozzles 2 and 3 as the CDRM cracks grew, the leak rate increased, and the wastage cavity evolved.

We used a state-of-the-art computer CFD code (STAR-CD) to build a three-dimensional model of the region around CRDM Nozzle. The STAR-CD code is used to carry out CFD modeling in a wide variety of science and technology fields such as aerospace, automotive, biomedical, chemical reaction, environmental, marine, oil and gas, power generation including nuclear power, and turbo-machinery applications. A more detailed description of the code and its capabilities is provided in Appendix C.

In this case, the physical boundary of the model is the CRDM nozzle of interest – in this case Nozzle 3 – and the metal walls of the nozzle, annulus, wastage cavity, and the space between the RPV head and the mirror insulation. The input flow stream to the model is the leak flow through the CRDM nozzle and weld cracks.

The physical volume of the model is divided into "cells", small control volumes that together make up the overall model. The models used for the smaller wastage cavity at Nozzle 2 and the final large wastage cavity at Nozzle 3 are shown in Figures 9.1 and 9.2. The smaller cavity used approximately 750,000 cells, while the larger cavity model used approximately 1.5 million cells. Each model run takes several days to run and converge on a steady state solution using several state-of-the-art workstations.

Within each of these cells, the basic physical laws governing mass, energy, and momentum conservation and transfer are applied to calculate the thermal hydraulic parameters such as velocity, temperature, pressure etc., of both the continuous phase (steam/air) and the dispersed (water droplet) phase. Heat transfer is allowed between the fluid streams and the metal walls that represent the physical boundaries of the model within which the fluid streams are constrained to flow.

The CFD code was used to determine the local fluid conditions - fluid velocity, temperature, pressure, moisture content, oxygen concentration, etc. - that exist throughout the modeled control volume as the defined CRDM nozzle leak flow exits the crack, travels through the annular crevice between the nozzle and the low-alloy steel portion of the RPV head, through whatever wastage cavity is being modeled, and exits into the space between the RPV head and the mirror insulation.

These fluid conditions are dictated by the underlying physics of the CFD code, and provide the basis for our evaluation of the potential for various metal removal and degradation mechanisms that resulted in the formation of the wastage cavity near CRDM Nozzles 2 and 3.

9.4 Leak Rate vs. Crack Length Calculations

Before we could begin the CFD modeling of the environmental conditions present in the annulus and wastage cavity at a cracked CRDM nozzle, we neeed to establish the relationship between PWSCC crack length and crack leak rate. Our initial effort to evaluate the leak rate from CRDM nozzle PWSCC cracks began with a review of the calculations completed by Dominion Engineering, Inc., shown in Figure 9.3.[6, 7]

These results, which show calculated leak rates for crack lengths ranging up to 1.6 inches, were based upon available data obtained for fluid leakage through thin-walled steam generator tubes. Based upon these results, the Root Cause Report attempted to compare the leak rates from the CRDM nozzle cracks identified by UT examination of Nozzles 2 and 3. The FENOC Root Cause Report noted: [8]

> "Length of Cracks in Davis-Besse Nozzles 2 and 3
>
> The longest crack lengths above the top of the J-groove weld determined by UT measurements are 1.1" for nozzle 2 and 1.2" for nozzle 3. The longest cracks above the J-groove weld previously discovered in other plants with low observed leakage are <1.0 inch. Since the Davis-Besse cracks are longer than in other B&W design plants, higher leak rates would be expected."

Based upon the observation of the head wastage that occured near Nozzle 2, the higher leak rates expected for the 1.1 inch long crack in Nozzle 2 did not occur. Our evaluation of the UT data shows that although the Nozzle 2 crack did extend 1.1 inches above the J-groove weld, the actual effective leak path length was only 0.24 inches. The details of the evaluation of effective leak rates for the longest cracks in Nozzles 2 and 3 were presented in Section 8.4.1.

The DEI leak rate calculations were completed using a finite element model (ANSYS) that determined the crack opening displacement under operating temperatures and pressures. Due to the assumptions and mechanism evaluated in this study, the results of these calculations, which are presented in Figure 9.3, significantly overestimate the leakage rate for all crack lengths. Two separate calculations, with and without the presence of the large wastage cavity in the RPV head, were completed.[9]

Both of these calculations over-estimate the crack leakage rates for the crack lengths observed in the Davis-Besse CRDM nozzles. An analytical solution to the crack leakage rate problem, completed by Zahoor, is also included in Figure 9.3. Neither the DEI calculations nor the Zahoor results accurately describe the leak rate as a function of crack length for thick-walled CRDM nozzles.

Using the historical unidentified leak rate data, we estimated in Section 7.2.1 that the total leak rate that could be attributed to all CRDM nozzle cracks at the end of Cycle 13 to be approximately 0.17 gpm. Based upon our evaluation of the existing CRDM crack leak rates, we undertook additional fluid modeling calculations of the leak rate for various crack lengths and compared these results with the range of measured unidentified leak rate during Cycle 13 at Davis-Besse.

At the end of Cycle 13, a number of cracks in CRDM Nozzles 2 and 3 were large enough to have leakage. In order to properly attribute the appropriate fraction of the total leakage to each nozzle crack, we completed a detailed calculation of the leak rate as a function of crack length for the specific geometry and conditions present at the Davis-Besse nozzles. The details of these calculations are summarized below and described in detail in Appendix D.

We used a three-step process to determine the flow rate through the crack:

1. Determination of pressure drop and velocity through an ideal nozzle.

2. Determination of the effective cross-sectional area of the crack.

3. Determination of a discharge coefficient relating the flow rate through the actual crack to the flow rate through an ideal nozzle.

The first step was to evaluate the thermodynamic conditions that would be present due to RCS fluid flowing through a CRDM nozzle crack. Based on the temperatures and pressures associated with these conditions, we calculated the velocity resulting from the pressure drop across the nozzle crack. We then estimated the cross sectional area of the crack based upon our knowledge of PWSCC crack dimensions. Finally, we evaluated a discharge coefficient for flow through cracks in thick-walled tubes that related the effects of actual crack geometry on the flow rate through the crack. Details of these calculations are presented in Appendix B.

The results of these leak rate calculations for fluid flow through CRDM PWSCC cracks are presented in Figure 9.4. This figure provides a comparison of leak rate vs. crack length for an ideal nozzle crack and cracks using more realistic flow conditions through thick-walled tubes. Using the effective crack lengths calculated in Section 8.4.1 of this report, an estimate of the leak rate for each of the various crack lengths in CRDM Nozzles 2 and 3 was obtained. Based upon the actual crack lengths for the Nozzle 2 and Nozzle 3 cracks, we estimated that the total leak rate through these cracks near the end of Cycle 13 was about 0.03 gpm. Since the total leakage ascribed to nozzle cracks in Section 7.2.1 was 0.17 gpm, there was a significant fraction of leakage (0.14 gpm) that was flowing through the only other observed flow path, the J-groove weld crack at Nozzle 3.

Our evaluation of the cracking observed in Nozzles 2 and 3, as discussed in Section 8.4.1, and the detailed metallurgical analyses of the nozzle cracks and the J-groove weld crack at the 10° location in Nozzle 3, show that the crack morphologies for the nozzle cracks and the J-groove weld crack are significantly different. Metallurgical examination of the top portion of the crack located at the 180° position in Nozzle 3 showed that the nominal crack width for this PWSCC crack was approximately 20 μm (0.0008 inches) as shown in Figure 9.5.[10]

The J-groove weld crack morphology, as determined by metallurgical analysis, was significantly different from that of the CRDM nozzle cracks. The crack in the J-groove weld was found to be approximately 400 μm (0.016 inches) wide, as shown in Figure 9.6[11.] Hence, the J-groove weld crack was about 20 times wider than the CRDM nozzle crack. This larger crack width resulted in significantly larger leakage rates (0.14 gpm) through the J-groove weld crack once the weld crack was uncovered by the growth of the wastage cavity as describe in Section 9.3.

The calculated leak rates vs. crack lengths for the J-groove weld crack for three crack widths 10 times, 15 times and 20 times wider than a CRDM nozzle PWSCC crack are shown in Figure 9.7. These relative crack widths are similar to those noted in Figures 9.3 and 9.4. As we describe in the sections that follow, the uncovering of the pre-existing crack in the J-groove weld by cavity wastage in October-November late in Cycle 13 caused a dramatic and abrupt increase in the leakage rate, and the development of fluid conditions that resulted in accelerated alloy steel removal from the RPV head.

9.5 Development of the Initial Wastage Cavity in the CRDM Nozzle Annulus

One of the difficulties in CFD modeling of the nascent birth of the wastage cavities at Nozzles 2 and 3 is the unknown state of the interference fit between the CRDM nozzles and the bore hole in the RPV head. The CRDM nozzles were installed with an interference fit that was achieved by machining the nozzle OD slightly larger than the bore hole, cooling the nozzle in liquid nitrogen, inserting it in place, and allowing the nozzle to warm back up to ambient temperature.

As we discussed in Section 7.1.2, four of the center CRDM nozzles at Davis-Besse (Nozzles 1, 2, 3 and 4) were predicted to retain an interference fit even under operating conditions, and this led to an NRC concern in late 2001 about whether through wall cracks in one of these four nozzles would be detectable by means of visual inspection for boric acid leakage.

The interference fit prediction was based on manufacturing records of measurments made at the top and bottom of the nozzles and the RPV head boreholes. While we have no reason to doubt the readings taken, we do not believe that the interference fit, even if it was calculated to be retained under operating conditons, could provide a "seal" against leakage as the NRC apparently was concerned it could.

First, metal-to-metal contact on a 4-inch diameter nozzle is certainly not perfect throughout the entire nozzle/borehole contact area, and at the microscopic level is more like one of "hills and valleys". Thus, flowpaths for water/steam leakage will always exist from the bottom of the annulus to the RPV head no matter what the calculated interfence fit, and in this we agree with the FENOC root cause report that a cracked nozzle will always result in boric acid leakage even with a predicted interfence fit[7][12]

Second, both Davis-Besse Nozzles 2 and 3 undoubtedly "leaked" boric acid, despite their nominal interference fit, so clearly flow paths existed from the leak location at the bottom of the annulus to the RPV upper head, otherwise no leakage and no wastage would have occurred.

The question then is one of how to predict exactly where a wastage cavity will begin to form as a result of leakage from an axial nozzle crack? In the case of the large wastage cavity at Davis-Besse Nozzle 3, the answer seems obvious – right above the longest crack that began to leak first. Since Nozzle 3 only had the one long axial downhill crack around 3^{o} at the top of the weld that leaked more than a trivial amount[b], that is where one would expect the wastage cavity to form, and that is where it did initially form and develop.

In the case of Davis-Besse Nozzle 2, the answer is not so obvious. Nozzle 2 had a total of seven axial cracks, six of which were through wall and one of which had a leak path around the weld (see Section 8, Table 8.1 and Figure 8.7). One would expect, based on

[b] The uphill crack at Nozzle 3 at 180^{o} did not reach a length above the weld where it could leak more than a miniscule amount, if at all.

the Nozzle 3 cavity location, that the wastage cavity at Nozzle 2 would begin to form above the one or more cracks that were the longest and therefore began leaking first.

At first glance, this would appear to be Crack 8, measured by UT to be 1.15 inches in length above the weld, with the top of the crack just below the bottom of the small wastage cavity at Nozzle 2 at the 270º location (see Figures 10.6 and 10.7). However, this reported length is misleading, and our analysis of this crack in Section 8.4.1 shows that it had an effective leak path length of only 0.24 inches, and likely leaked at a miniscule rate or not at all.

The other two cracks in Nozzle 2 either side of the bottom of the wastage cavity were Cracks 6 and 10, and these two cracks only had effective leak path lengths above the weld of 0.57 and 0.46 inches respectively (see Figures 8.7 and 10.6 again), and again likely leaked only miniscule amounts.

The two longest leaking cracks at Nozzle 2 in February 2002 were Cracks 2 and 13, with effective leak path lengths above the weld of 0.82 and 0.76 inches respectively (see Figures 8.7 and 10.6 again), which certainly were the first cracks in Nozzle 2 to begin leaking. Yet these two longest cracks in Nozzle 2 are on either side of the 90º location, 180º around the nozzle from the wastage location. So how did the the wastage cavity, undoubtedly caused by these two far away cracks, get started where it did?

We believe that the answer to this apparent conundrum lies in the variable interference fit. When a crack first begins to leak, the leak flow will find its way through the path of least resistance – the widest path with the greatest clearance - to the top of the annulus. Flashing will occur along this leak path wherever the leak flow encounters the first region of somewhat “looser” interference fit - and therefore low pressure - that is connected to the top of the annulus at the RPV head.

Because there is no data that provides even a hint as to where this location might be in a given nozzle with a random and indeterminate interference fit, we have no option but to accept that for Nozzle 3, it was right above the only leaking crack, and that in Nozzle 2, it was some 180º away from the two major leaking cracks.

Our CFD modeling indicates that once a wastage cavity got started, annulus and cavity enlargement by the processes described in Section 9.6 would ensure that it remains anchored wherever it initiated.

Because the initial location of the incipient cavity is unpredictable, we have not attempted to model it. We assumed that the cavity got started where it did for the reasons outlined above, and we started our modeling efforts with a small wastage cavity at that location.

This discussion serves to highlight the fact that the large wastage cavity at Davis-Besse Nozzle 3 was truly a unique "one of a kind" event. First, Nozzle 3 had highly susceptible Alloy 600 material that exhibited crack growth rates higher than previously analyzed or predicted, thereby causing the longest CRDM nozzle crack ever discovered.

Second, the leakage from this fast-growing crack, which could have started a wastage cavity in another location away from the crack as occurred in Nozzle 2, actually started a wastage cavity directly above the crack location, such that the upward growing crack had the shortest possible path to the downward growing wastage cavity.

Third, the very high crack growth rate caused the crack to reach a critical length and begin leaking at a critical rate into the wastage cavity in an unexpected and unpredictably short period of time – a matter of a few months.

Fourth, a through wall axial weld crack rapidly grew in the same coincident location as the axial nozzle crack, such that when the wastage cavity growth downward accelerated in October-November 2001, the wide weld crack was waiting to be exposed and substantially increase the leak rate, causing the large wastage cavity to grow at Nozzle 3 in a matter of a few months during the October 2001 to February 2002 time frame.

9.6 CFD Modeling of the Initial Stages of Wastage Cavity Growth at CRDM Nozzles 2 and 3

The major undertaking in the analysis required to evaluate the environmental conditions conducive to material degradation was the construction of a detailed computational fluid dynamics (CFD) model of the initial wastage states that develop as the crack leakage

increases. CFD modeling was used to identify the development of environmental conditions that resulted in the formation and growth of the wastage cavity that was discovered during 13RFO adjacent to Nozzle 2, as well as what we have concluded were the initial stages of the development of the large wastage cavity discovered at Nozzle 3.

9.6.1 Input and Boundary Conditions

The CFD model is described in Section 9.3.2 and in more detail in Appendix C. The model accounts for the fact that, due to its temperature and pressure, the leak flow through the crack, which is subcooled water at RCS conditions of 2155 psig and 605°F, will quickly expand and partially flash to steam after exiting the crack as it flows into the lower pressure region of the annulus and wastage cavity. This expansion causes a rapid acceleration of the fluid. The phase change from water to steam results in an increase in fluid volume that causes a significant increase in fluid velocity at, or just down-stream of, the area of greatest flow restriction.

Thermodynamic conditions dictate that only a portion of the leaking RCS fluid flashes to steam as it exits the CRDM crack. Approximately 35% of the fluid flashes to steam under most flow conditions. The remaining 65% of the fluid remains as liquid water droplets, which are accelerated by the expansion of the flashing steam to very high velocities (~ 2,000 fps) near the crack.

Further acceleration of the fluid can occur “down stream” of the crack as changes in the geometry of the system (annulus size, wastage cavity formation, etc) permit additional expansion of the fluid. Also, as the fluid flashes to steam, a significant amount of heat is transferred from large mass of the surrounding RPV head steel that results in some cooling of the metal surfaces near the flashing fluid stream.

The three dimensional CFD modeling runs for fluid flow in the region adjacent to CRDM Nozzle 3 were completed for a crack located at approximately 10 degrees clockwise of the “downhill” direction (toward Nozzle 11). This location is consistent with both the major leaking axial crack identified in the J-groove weld by metallurgical examination, and the above weld axial nozzle crack identified by UT examination of the nozzle and at the same locations.

Input and boundary conditions were specified for the CFD modeling runs for three separate combinations of nozzle axial crack length[c] and leak rate, wastage cavity size, and relative axial position of the bottom of the wastage cavity and the top of the crack. The CFD modeling runs covered a range of crack lengths (0.5, 0.8, and 1.0 inches) together with the associated leak rates from Section 9.3 (0.001, 0.01, and 002 gpm), and two different wastage cavity sizes.

The CFD modeling runs used two representative cavity geometries representative of the wastage cavity development at Nozzles 2 and 3. The first cavity geometry, which was used for the 0.5-inch and 0.8-inch CRDM nozzle cracks, represents the conditions prior to the wastage cavity growing downward to the point where it intersected the upward growing axial nozzle crack. This geometry is similar in shape to the wastage cavity found near Nozzle 2 at 13RFO, and represents a "known" cavity that formed in the Nozzle 2 annulus as a result of cracks for which the calculated leak rates were similar to those expected for the 0.5-inch and 0.8-inch cracks employed in these model runs.

The second cavity geometry, which is somewhat larger than the first, was defined to represent the case where the crack has grown up the CRDM nozzle to such a length, and the wastage cavity has expanded down through the alloy steel RPV head toward the J-groove weld to such a depth that the crack begins leaking directly into the wastage cavity.

The annulus geometry modeled in these runs was set at a 0.002 inch (2 mil) radial gap over an arc length of 0.5 inches with the crack centered on this arc (Cases 1 and 2). While this is somewhat arbitrary, as we discussed in Section 9.5, there is no basis on which to accurately model the variable interference fit initially present in the annulus. Therefore, the annular flow area was set small enough to be representative of the initial annulus, as well as to provide restriction to the leak flow. The same radial gap in the annulus (0.002 inch) with an arc length of 1.6 inches was used to model the conditions as the wastage cavity grew larger (Case 3).

---

[c] Throughout this section we use the short term "crack length" synonymously with the "effective crack length for leakage" term that we defined in Section 8.4.1.

The following three cases were defined and CFD modeling runs were completed for each case.

Case 1: For this case, the leak flow was 0.001 gpm (525 gal/year) from an axial nozzle crack extending 0.5 inch above the weld, with the bottom of the wastage cavity located 1.9 inches above the top of the crack. The leak flow and nozzle crack location are representative of the likely leak flows and crack locations at Nozzle 3 in May 2000, as well as the likely leak flow at Nozzle 2 around May 2001. For the initial run for this case, the wastage cavity was set equal to the size of the wastage cavity found at Nozzle 2 in March 2002. Since the leak flow for this case is very low, the results are dominated by the annulus restriction between the top of the crack and the bottom of the wastage cavity, and are insensitive to the size of the wastage cavity.

Case 2: As for Case 1, the wastage cavity was set equal to the size of the wastage cavity found at Nozzle 2 in March 2002. The leak flow was 0.01 gpm (5,250 gal/year) from an axial nozzle crack extending 0.8 inch above the weld, with the bottom of the wastage cavity located 1.6 inches above the top of the crack. The cavity size and shape, leak flow, and nozzle crack location are representative both of the terminal state of the cavity at Nozzle 2 in February 2002, as well as the likely state of the wastage cavity, leak flow and nozzle crack location at Nozzle 3 prior to May 2001, before the axial nozzle Crack 1 at Nozzle 3 grew upward into the downward growing wastage cavity.

Case 3: For this case the leak flow was 0.02 gpm (10,500 gal/year) from an axial nozzle crack extending 1.0 inch above the weld, with the top of the crack located 0.2 inches above (and into) the bottom of the wastage cavity. The wastage cavity was set equal to seventimes the size of the wastage cavity found at Nozzle 2 in March 2002, i.e., a later stage of cavity growth than Cases 1 and 2. This case is representative of the cavity, leak flow and nozzle crack location for Nozzle 3 after May 2001 but before October-November 2001, i.e., prior to the weld crack uncovering at Nozzle 3.

The results of the CFD modeling runs for these three cases, which were selected to assess the evolution of the wastage cavity at Nozzle 2 and at Nozzle 3 up to the point of uncovery of the weld crack, are presented in Sections 9.6.2, 9.6.3 and 9.6.4 below. The

results of these CFD modeling runs are the fluid parameters of temperature, pressure, velocity, steam quality (dryness), and oxygen content for the flow stream from the time it exits the crack until it escapes the CFD system boundary in the air-space region between the RPV head and the mirror insulation.

The CFD model output itself is a three dimensional output for each cell in the model structure (see Section 9.3.2) for the fluid parameters of interest for both the continuous phase (steam, air) and the dispersed phase (water droplets), which uses between 750,000 and 1.5 million cells. In the sections that follow, we have chosen to present the key parameters in more simple 1-dimensional plots along the crack length, annulus and wastage cavity. These plots highlight the important fluid conditions that are critical to assessing the potential for the various metal removal mecahnisms that we identified and discussed in section 9.2. Sets of color coded 2-dimensional "slices" through the regions of interest for each case are included in Appendix D.

The CFD modeling results have provided considerable insights into the development of thermal hydraulic conditions in the annulus and wastage cavity as the leak rate from growing cracks increased, and two results are of particular significance.

The first is that the CFD modeling identified very high fluid velocities at various locations that are dependent on crack length, leak rate, annulus and cavity geometry, and the relative axial locations of the crack and wastage cavity. These high velocities are a result of first, the flashing of the initially sub-cooled primary coolant liquid stream at 605ºF into a high velocity atomized steam/water stream as it exits the crack, and second, the acceleration of the resultant flow stream as it both expands into lower pressure regions and as the remaining liquid water is evaporated by heat transfer from the hot metal surfaces. This is an important result, since as described in Section 9.2, high velocities by themselves can not only cause metal removal at significant rates, but also are integral to the flow assisted corrosion (FAC) mechanism of metal removal.

The second is that the CFD modeling identified specific regions of temperature sufficient to result in the phase transformation of orthoboric acid to metaboric acid, and again these were found to be dependent on crack length, leak rate, annulus and cavity

geometry, and the relative axial locations of the crack and wastage cavity. In conjunction with fluid stream conditions where droplets of mositure are still present, i.e., where the vapor phase is still wet, both conditions conducive to accelerated corrosion by re-wetted molten boric acid are created.

9.6.2 CFD Case 1 – Crack Length of 0.5 Inch, Leak Rate of 0.001 gpm, Bottom of Wastage Cavity 2 Inches Above Top of Crack

In May 2000, the downhill crack at Nozzle 3 was estimated from the crack growth analysis in Section 8 to have grown to a point where the effective leak length above the weld was about 0.5 inch. This crack length is close to the length below which PWSCC cracks are thought to allow miniscule leakage, and the leak rate for this crack length was estimated from Section 9.4 to be 0.001 gpm (525 gal/year). Since the leak rate of 0.001 gpm for this model run was also equivalent to the leak rate estimated for all of the cracks combined at Nozzle 2 in May 2001, we also consider this case to also be representative of the state of the Nozzle 2 cavity at that time.

Since this leak rate is only 10% of the leak rate estimated for all the cracks combined at Nozzle 2 in February 2002, it is highly likely that the wastage cavity at Nozzle 3 in May 2000 was in the early stage of growth, and that it was much smaller than the cavity eventually found at Nozzle 2 in February 2002. However, since the leak flow for this case is very low, we expected that the results would be dominated by the annulus restriction between the top of the crack and the bottom of the wastage cavity, and would be insensitive to the size of the wastage cavity itself. Therefore, for the initial run for this case, the wastage cavity was set equal to the size of the wastage cavity found at Nozzle 2 in March 2002, with the bottom of the cavity located well above the top of crack.

The average velocity and the maximum velocity for the fluid stream exiting the 0.5-inch nozzle crack as a function of distance above the J-groove weld are shown in Figure 9.8, together with the relative size and location of both the nozzle cavity and the crack. The results show that the average velocity for the entire mass of fluid is less than 100 fps (68 mph) and decreases as the fluid enters the small wastage cavity located approximately 1.9 inches above the top of the crack.

While the maximum fluid velocity over the length of the crack is over 2,000 feet per second (fps), (1,360 mph), the full 3-dimensional results show that this maximum velocity is confined to the region close to the crack exit. This maximum velocity is close to the velocity at which metal removal by steam/water jet cutting can occur, and so some localized annulus enlargement could have occurred in the region of the crack exit.

Figure 9.9 shows the pressure as a function of distance above the J-groove weld, as can be seen, for this low leak rate, even the assumed tight annulus clearance does not result in any back pressure in the region of the crack exit.

The most important results for this case are the area-average annulus and cavity wall temperatures shown in Figure 9.10, and the average fluid steam quality shown in Figure 9.11, again both as function of distance above the J-groove weld. The wall temperatures indicate the cooling effect of even this very low leak rate on the wall of the annulus below the wastage cavity.

As the fluid exits the crack and flashes to steam, the area-average wall temperature within the annulus is predicted to drop to around 330°F. As the fluid travels up the annulus (to the right on the figure), the temperature remains relatively constant as the liquid portion of the fluid stream continues to evaporate into steam due to heat transfer from the hot metal surface of the annulus and CRDM nozzle wall. At the low leak rate of 0.001 gpm, the steam quality of the fluid stream is high throughout the annulus.

The average wall temperature in the annulus indicates that evaporation is essentially complete before the fluid exits the annulus into the wastage cavity, at a point predicted by the model to be approximately 1.5 inches above the weld where the wall temperature rapidly rises to around 450°F. As the fluid enters the small wastage cavity, the surface area for heat transfer increases and the average wall temperature rises to a maximum of approximately 600°F until it exits the wastage cavity at the top. At a temperature of 336°F, dehydration and phase transformation from orthoboric to metaboric acid takes place, and at 457°F, metaboric acid begins to melt. At the wall temperatures predicted to exist both in the upper region of the annulus and in the wastage cavity, the phase transformation of boric acid into metaboric acid would almost certainly occur, although

it is also likely that boric acid crystals would form in the fluid vapor stream and be carried out with the flow.

While solid metaboric acid could possibly be deposited in the lower region of the annulus, it is only at the very top of the annulus and in the wastage cavity itself that the temperatures are predicted to be high enough to melt these deposits. However, the dry conditions throughout the annulus and wastage cavity also indicate that when the leak rate is very low, the water droplets in the fluid stream are essentially quickly evaporated, and so corrosion due to re-wetted molten metaboric acid is unlikely.

Overall, the potential for metal removal by either mechanical steam/water jet cutting or boric acid corrosion is small, and annulus enlargement and wastage cavity growth rates will be low as long as the leak rate remains at this very low level and the annulus and cavity remain dry.

9.6.3 CFD Case 2 – Crack Length of 0.8 Inch, Leak Rate of 0.01gpm, Bottom of Wastage Cavity 1.7 Inches Above Top of Crack

The wastage cavity for this modeling run was set equal to the size of the wastage cavity actually found at Nozzle 2 in March 2002, and the analysis in Section 9.4 shows that the combined leak rate from the all of the cracks found at Nozzle 2 at that time was around 0.01 gpm (5,250 gal/year). Also at that time, the bottom of the wastage cavity at Nozzle 2 was still well above the top of the longest axial nozzle crack.

In April-May 2001, the crack growth rate analysis in Section 8 shows that the downhill crack in Nozzle 3 was around 0.87 inches in effective leak length, with an estimated leak rate of about 0.007 gpm (3,700 gal/year). Since this leak rate is slightly less than the 0.01 gpm used for this modeling run, it is likely that the wastage cavity at Nozzle 3 in April-May 2001 was somewhat smaller in size than the wastage cavity actually found at at Nozzle 2 in March 2002. We therefore consider this modeling run output to be representative of the conditions in the wastage cavity at Nozzle 3 in April-May 2001, i.e. at a point in its development where the upward growing axial nozzle crack had not yet reached the bottom of the downward growing wastage cavity.

Since the leak rate for this model run was ten times that for Case 1, both the average and maximum fluid velocities are much higher, as shown in Figure 9.12. The average velocity in the annulus exceeded 500 fps (341 mph) from the top of the crack to the bottom of the wastage cavity, and the maximum fluid velocity just slightly above the top of the 0.8-inch crack exceeded 2,200 fps (1,500 mph). The maximum fluid velocity also remained between 800 fps and 1,100 fps (545 mph and 750 mph) in the annular region below the small wastage cavity. Upon reaching the wastage cavity, both the average velocity and the maximum fluid velocity decreased considerably due to the expansion of the fluid stream into the larger cavity volume.

As for Case 1, the maximum velocity in the annulus region close to the crack is close to the velocity at which metal removal by steam/water jet cutting can occur (see Appendix D), and so again some localized annulus enlargement due to mechanical metal removal could have occurred in the region of the crack exit.

Figure 9.13 shows the pressure as a function of distance above the J-groove weld. The combination of the higher leak flow with the same assumed annulus dimensions for this case results in the development of a back pressure at the bottom of the annulus predicted to be around 45 psi. However, this is well below the pressure level that would affect the leak flow through the crack, and indicates that even the assumed tight annulus condition does not have a significant effect.

The model results for the area average metal wall temperature are somewhat different from those for the lower leak flow used in Case 1. As shown in Figure 9.14, due to the higher leak rate flow, the area-average wall temperature adjacent to the crack is predicted to be around 300°F. The wall temperature slowly increases as the fluid travels up the annular region towards the wastage cavity, and is predicted to reach around 380°F to 400°F at the top of the annulus.

The much larger metal surface area for heat transfer in the wastage cavity then results in a rapid increase in area average wall temperature to around 500°F. Thus, while wall temperatures high enough to result in the phase transformation of orthoboric to metaboric acid (at 357ºF) are predicted to occur in the upper section of the annulus,

melting of the metaboric acid (at 457ºF), is not predicted to occur until the fluid stream exits into the bottom of the wastage cavity and contacts the hotter metal surfaces there.

The most marked difference from the Case 1 results lies in the results for steam quality. The model results in Figure 9.15 show that while dryout of the fluid stream begins down in the annulus (steam quality increasing), moisture persists and steam quality in the vapor stream does not reach 1.0 (i.e. dryness) until the fluid stream is well up into the wastage cavity. Thus, moisture in the form of atomized water droplets is predicted to be present in the fluid vapor stream throughout the annulus and in the bottom of the wastage cavity. Any pre-existing or newly-deposited molten metaboric acid would become highly corrosive to the low alloy steel RPV head material in the presence of moisture. Flow assisted corrosion is also possible in these regions, especially the annulus, due to the high average and local maximum velocities.

The location where the CFD results predict the simultaneous occurrence of both wall temperatures in excess of the melting point of boric acid and the presence of moisture is at the bottom of the wastage cavity. In addition, high average and maximum velocities persist in this same region.

Thus, the significant consequence of the increasing leak rate to around the 0.01 gpm level, in conjunction with the expected sub-surface wastage cavity size, is predicted to result in thermal hydraulic conditions where the metal removal process at the bottom of the wastage cavity and possibly in the top of the annulus shifted from relatively slow localized metal removal by steam/water jet cutting, to a combination of this mechanical removal with aggressive corrosion due to re-wetted boric acid and flow assisted corrosion.

Overall, the combination of these factors would result in an acceleration of the growth rate of the cavity downward toward the upward growing CRDM nozzle crack. For the growing wastage cavity at Nozzle 3, this point was reached some time around April-May 2001. It is likely no coincidence that at this time the frequency of containment air cooler cleaning due to boric acid contamination rapidly decreased to zero.

9.6.4 CFD Case 3 – Crack Length of 1.0 Inch, Leak Rate of 0.02 gpm, Bottom of Wastage Cavity 0.2 Inches Below Top of Crack

The CFD run for this case was based on a much larger wastage cavity about seven times the size of the wastage cavity found at Nozzle 2 in March 2002, i.e. at a later stage of cavity growth at Nozzle 3 than for Cases 1 and 2. For this case the leak flow was set higher at 0.02 gpm (10,500 gal/year) from an axial nozzle crack extending 1.0 inch above the weld, with the top of the crack located 0.2 inches above (and into) the bottom of the larger wastage cavity. We believe that this is representative of the cavity, leak flow and nozzle crack location for Nozzle 3 after May 2001 but before October-November 2001, i.e., prior to the weld crack uncovering at Nozzle 3.

The growth of the top of the crack into the wastage cavity results in major changes in all of the thermal hydraulic conditions that can cause extremely rapid metal removal rates.

First, as shown in Figure 9.16, the average fluid velocity is similar to Case 2, with the mass average velocity increasing to 620 feet per second near the top of the annulus 0.8 inches above the weld, then dropping off rapidly as the fluid stream from the annulus enters the larger wastage cavity.

However, Figure 9.16 also shows that very large maximum velocities of approximately 2,700 fps (about 1,800 mph) develop in the lower part of the wastage cavity where the top of the crack extends above the bottom of the cavity. In addition, the direction of the high velocity steam/water mixture is radially outward toward the cavity wall, resulting in direct impingement of this part of the leak flow on the bottom of the cavity wall that is in close proximity to the crack. This is in contrast to Cases 1 and 2, where the leak flow is turned into the axial direction by the tight annulus gap.

Impingement tests using nozzle jets of high temperature boric acid on carbon steel surfaces conducted both before 2002 (Section 6.3.1) and as part of the EPRI corrosion test program after 2002 (Section 6.4.1) showed that penetration rates of up to 11 inches/year can result at the impingement location when the metal surface is in close proximity to the jet nozzle. In addition, these extremely high fluid impingement

velocities can cause material removal rate at a high rate as a result of mechanisms such as water jet cutting and abrasive water jet cutting (Section 9.2).

Figure 9.17 shows the pressure as a function of distance above the J-groove weld. As for Case 2, the higher leak flow of 0.02 gpm with the same assumed annulus dimensions again results in the development of a back pressure at the bottom of the annulus predicted to be around 40 psi. However, as for Case 2, this is well below the pressure level that would affect the leak flow through the crack, and again shows that even the assumed tight annulus condition does not have a significant effect. The model results for the area average metal wall temperature are different from those in Cases 1 and 2. As shown in Figure 9.18, the metal wall temperature in the annular crevice remains in the 280ºF to 330ºF range due to the higher leak rate flow. However, because of the large metal surface area in the larger cavity for this case, the metal wall temperature is predicted to be around 500ºF throughout the cavity.

Thus, wall temperatures high enough to result in first, the phase transformation of orthoboric to metaboric acid (at 336ºF), and second, melting of the metaboric acid (at 457ºF), do not occur until the fluid stream reaches the bottom of the wastage cavity.

The steam quality predicted for this case is also different from Case 2. As shown in Figure 9.19, due to the higher leak flow, the fluid stream stays wet throughout the annulus and significant moisture persists well into the wastage cavity. Moreover, even though dryout is predicted to begin in the wastage cavity, moisture persists all the way to the top of the cavity and the upper surface of the RPV head.

Since the boric acid on the RPV head surrounding Nozzle 3 is likely in the form of a layer of molten metaboric acid at the head temperature, at this leak flow, the penetration of some moisture to the upper head provides the combination of conditions for general corrosion of the upper head surface around Nozzle 3 by re-wetted molten metaboric acid.

Overall for this case, at the bottom of the wastage cavity extremely high maximum velocities, direct impingement of the leak flow, molten metaboric acid, and abundant moisture all combine to cause very high metal removal rates at this location due to all of

the mechanisms identified in Section 9.2. Thus the downward growth as well as the likely lateral enlargement of the cavity would all be expected to accelerate.

We believe that this accelerating downward growth of the wastage cavity at Nozzle 3 took place between May 2001 and October-November 2001. At that time, the step jump in unidentified leak rate discussed in Sections 7.2 and 9.4 indicates that the large weld crack at Nozzle 3 rapidly uncovered, resulting in a significant increase in leak rate

9.7 CFD Modeling of the Final Wastage Cavity at CRDM Nozzle 3

The CFD model was used to examine two cases using the actual wastage cavity size (195 cubic inches) and shape found at CRDM Nozzle 3 in March 2002:

Case 4: This case used the actual as-found wastage cavity geometry, with the axial crack in Nozzle 3 extending 1.23 inches above the weld (1.13 inch effective leak path length), and the axial crack in Nozzle 3 J-groove weld extending 0.7 inches radially across the weld. The total leak flow from the combined axial nozzle and weld cracks was set at 0.17 gpm - 0.03 gpm from the nozzle crack and 0.14 gpm from the much wider weld crack (see Section 9.4). This model run was made to gain understanding of the thermal hydraulic conditions and complex flow patterns that were present towards the end of Cycle 13 as the wastage cavity and leak flow were close to their final state.

Case 5: This was a transient analysis of Case 4 starting with the final wastage cavity filled with aqueous boric acid and starting injection of high velocity fluid at 0.17 gpm from the final CRDM Nozzle 3 cracks (nozzle crack and weld crack) into the cavity. This model run was undertaken to determine if it was possible, given the fluid velocities and flow patterns that develop, for aqueous boric acid to be retained in the final wastage cavity.

9.7.1 CFD Case 4 – Modeling of the Final Wastage Cavity at CRDM Nozzle 3 and Final Leak Rate in February 2002

This modeling run first required modeling of the volume and shape of the final wastage state, which included the 195 cubic inch cavity extending from the top of the RPV head

to the base of the stainless steel cladding between Nozzles 3 and 11. The crack in Nozzle 3 extended 1.23 inches above the J-groove weld (1.13 inch effective leak path length) and 0.7 inches through the J-groove weld. The total estimated leak rate, based partly on the unidentified leak rates late in Cycle 13, and on the calculated leak rates for the nozzle and weld cracks defined in Section 9.4, was 0.17 gpm (89,000 gal/yr).

The model results for this case are included in detail in Appendix C, and we present here just the more important features. The model results show that, starting near the crack, the sub-cooled water at 605ºF exits the cracks, changes phase to steam, expands, and rapidly accelerates. Slightly further away from the crack, the stream of water and steam expands into the open wastage space. Once the fluid hits the wall (the "nose") of the wastage cavity opposite the crack, it is redirected back around towards the nozzle, and then up and out of the cavity.

Figure 9.20 shows the velocity at a vertical cross section "slice" taken through the center line of the cracks in the nozzle and weld, all the way from the bottom of the wastage cavity up to the underside of the mirror insulation above the RPV head. High velocities of around 700 fps at the immediate crack exit rapidly dissipate, although relatively high fluid velocities of over 200 fps persist in the jet almost the length of the cavity, dropping to around 75 fps as the jet hits the cavity wall near the front "nose" of the cavity towards Nozzle 11.

The shape of the wastage cavity induces circulation patterns, which are evident in the velocity contours in Figure 9.20, thus air entrainment of hot air from above the head takes place into the wastage cavity. This would enhance corrosion of the RPV low alloy steel if concentrated boric acid solution were present in the wastage cavity.

Figure 9.21 shows the temperature contour, again on the same vertical cross section "slice" as Figure 9.20. The fluid stream in the wastage cavity is cooled to around 212ºF by expansion and flashing to the atmospheric pressure prevailing in the wastage cavity, and heat transfer form the cavity walls is insufficient to vaporize all the moisture in the leak flow. The metal surfaces of the wastage cavity remain hot, with some localized cooling directly opposite the crack exit as shown in Figure 9.22.

The underside of the boric acid layer on top of the RPV head, which was almost certainly partially molten metaboric acid, would be re-wetted by the exiting fluid stream, resulting in a high corrosion rate of the top steel surface of the RPV head at up to 6 inches/year. This corrosion would have progressed downward, both enlarging the upper portion of the cavity, and resulting in the smooth appearance of the steel surfaces in this region, as shown in Figures 9.23,[13] 9.24[14] and 9.25.[15-16]

9.7.2 CFD Case 5 – Transient Analysis of Fluid Flow and Fluid Ejection from the Final Wastage Cavity at CRDM Nozzle 3

The velocity profiles predicted by the Case 4 model runs suggested that the wastage cavity might be incapable of retaining a "pool" of concentrated aqueous boric acid. An additional CFD run was therefore completed to document the effect of the injection of high velocity fluid at 0.17 gpm from the final CRDM Nozzle 3 crack (nozzle crack and weld crack) into the final wastage cavity initially filled with concentrated boric acid solution. These transient calculations were completed to determine if general corrosion processes resulting from the formation and retention of a pool of saturated aqueous boric acid solution within the cavity caused a majority of the wastage cavity in the final stages, as suggested by the FENOC Root Cause Report (see section 9.1, "Stage 4").

The CFD model output results for the Case 5 transient analysis are presented in Figures 9.26 through 9.29. These figures present a top view and a perspective view of the final wastage cavity near CRDM Nozzle 3. Figure 9.26 shows the initial configuration with a pool of aqueous boric acid filling the cavity during time steps 0.001 seconds, 0.005 seconds, and 0.02 seconds. The darker blue area in each view represents a liquid vapor interface. For the three top views shown in Figure 9.26, the dark blue area represents the surface of the aqueous boric acid pool. For the three perspective views, the top surface of the pool and the interface between the boric acid pool and the steam/liquid mixture exiting the crack are evident. Note that the volume of the steam/liquid mixture exiting the crack increases as the time steps increase from 0.001 seconds to 0.02 seconds.

Figure 9.27 shows the progression of the transient for times from 0.05 seconds through 0.10 seconds. During this period, the steam/liquid mixture exiting the crack continues to grow in volume until it finally disrupts the surface of the aqueous boric acid pool.

Figure 28 shows the continued progression of the transient for times from 0.12 seconds through 0.20 seconds.

Significant disruption of the aqueous boric acid pool occurs. Liquid boric acid is rapidly ejected from the wastage cavity, and strikes the mirror insulation and support structures above the RPV head. Figure 9.29 shows the final time steps of the transient analysis (from 0.25 seconds to 0.40 seconds). The majority of the aqueous boric acid that originally resided in the wastage cavity has been ejected.

After striking the mirror insulation and its support structures, the ejected material is finally deposited behind Nozzle 3. The location of this deposit of aqueous boric acid predicted by the CFD model is the same as that of the boric acid and corrosion product deposits that were found on the RPV head at the 90 degree and 270 degree sides of Nozzle 3 (and between Nozzle 3 and Nozzle 1) in the RPV head inspection video completed after the hydro-lasing efforts during 13RFO (see Figures 7.15 and 7.16 in Section 7). The observed deposits confirm the trajectories predicted by the CFD model for material ejected from the wastage cavity by the high-velocity fluid stream exiting the cracks in the CRDM Nozzle 3 and weld.

Based upon the results of this transient analysis, we conclude that aqueous boric acid could not have been retained within the wastage cavity with a leak rate of 0.17 gpm, since the high velocity fluid stream would eject the aqueous boric acid solution from the wastage cavity.

However, orthoboric acid deposited on the hot metal walls of the wastage cavity would rapidly be converted into molten metaboric acid since the metal temperatures are above both the phase transition temperature of 336ºF and the meting point of 457ºF. Metaboric acid is significantly more viscous than concentrated aqueous boric acid and is therefore less likely to be ejected from the wastage cavity by the high-velocity fluid stream exiting the CRDM crack. Finally, as noted above in Section 9.7.1, molten metaboric acid in the presence of moisture would cause rapid corrosion of the alloy steel RPV head material.

9.8 Summary

Although the exact mechanism (or combination of mechanisms) that resulted in the formation of the wastage cavity on the Davis-Besse RPV head may never be precisely known, the knowledge that high fluid velocities and environmental conditions conducive to flow assisted corrosion or other mechanical material removal mechanisms suggest that the wastage cavity formed in a time period much shorter than the 4 year estimate in the Root Cause Report. Based on the results of our calculations and a review of recent technical literature, our best estimate is that the wastage cavity on the Davis-Besse RPV head formed late in Cycle 13, most likely between October/November 2001 and February 2002.

The results presented in this section show that the CRDM leak at Nozzle 3 resulted in a set of conditions that facilitated a number of different material removal mechanisms, each of which is more aggressive at different crack lengths, leak rates, and thermal conditions. A combination of the effects of these mechanisms caused the rapid formation of the wastage cavity in approximately five months or less. The speed with which the wastage cavity formed under these thermal fluid conditions highlights the unexpected and unforeseeable nature of this problem. It also points out that the formation of this wastage cavity was not part of the ordinary wear and tear expected in an operating PWR.

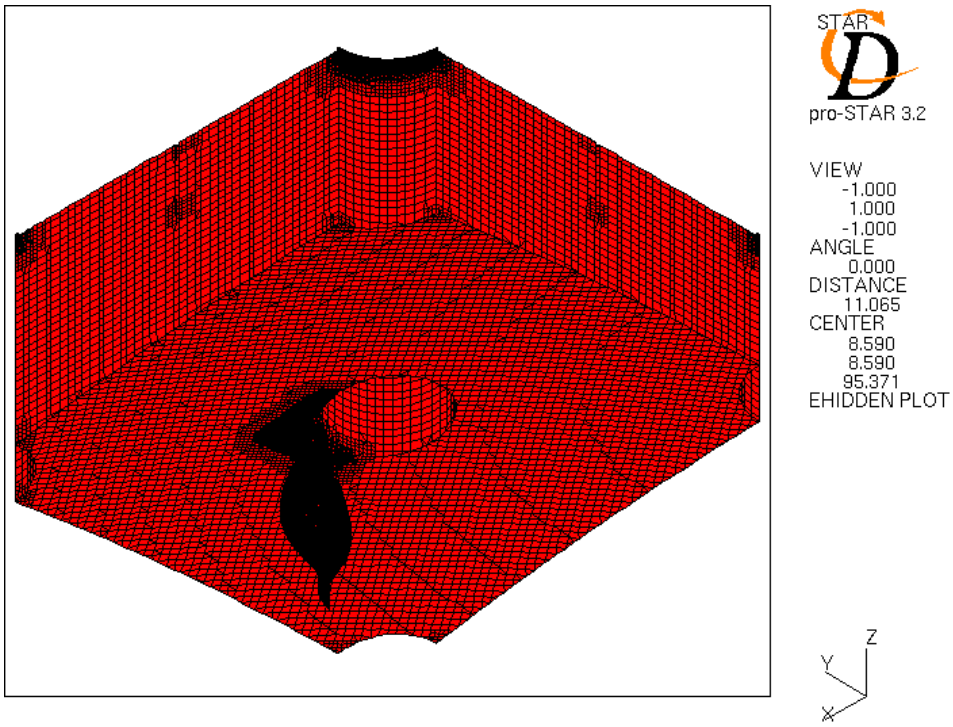

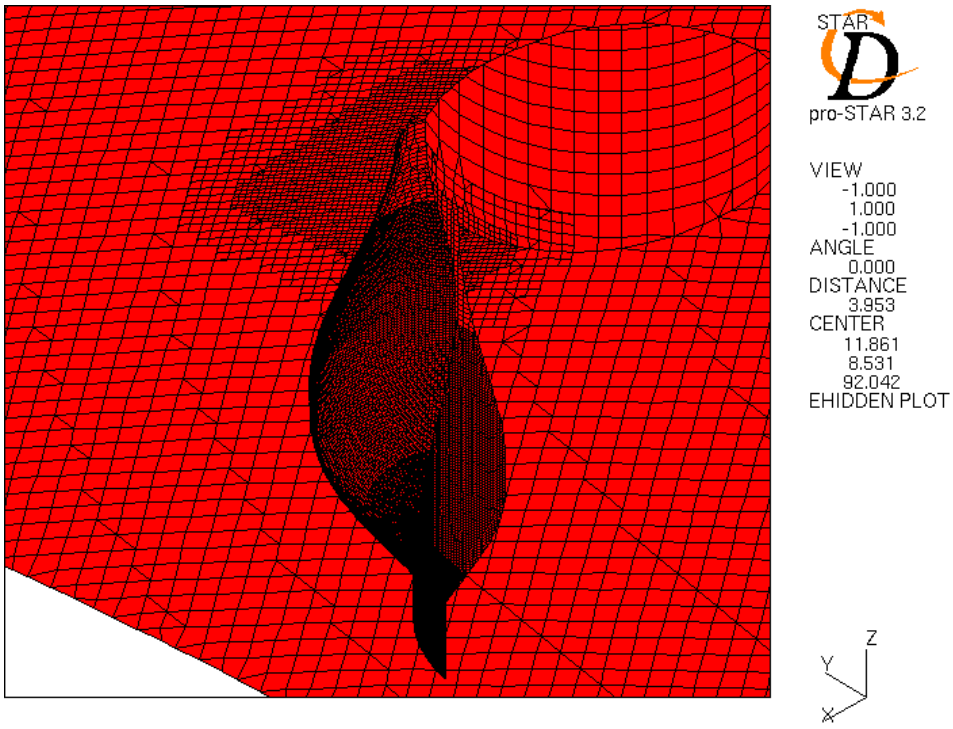

Figure 9.1(a) CFD Model Mesh for Case 3 Small Wastage Cavity

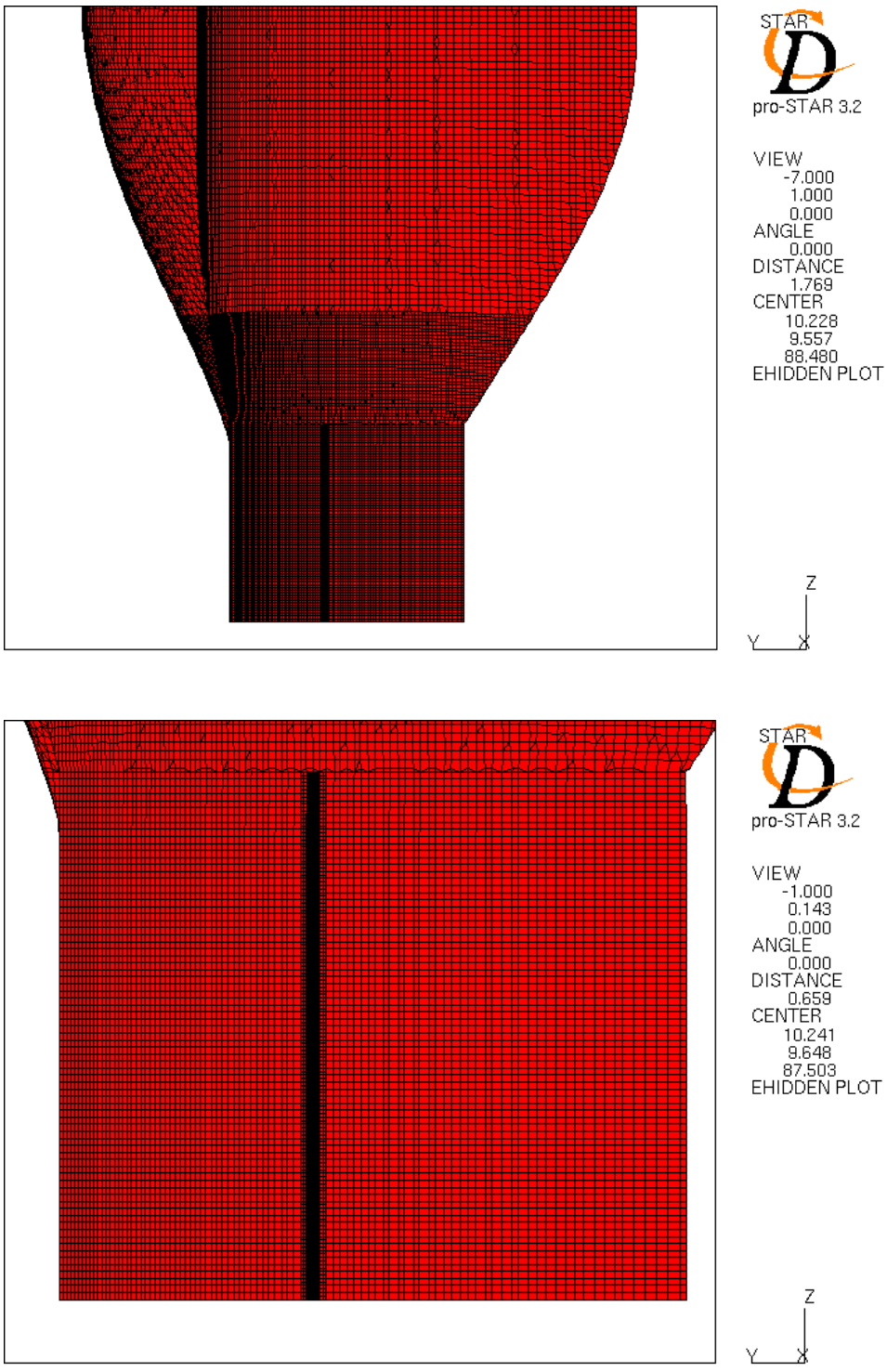

Figure 9.1(b) CFD Model Mesh for Case 3 Small Wastage Cavity

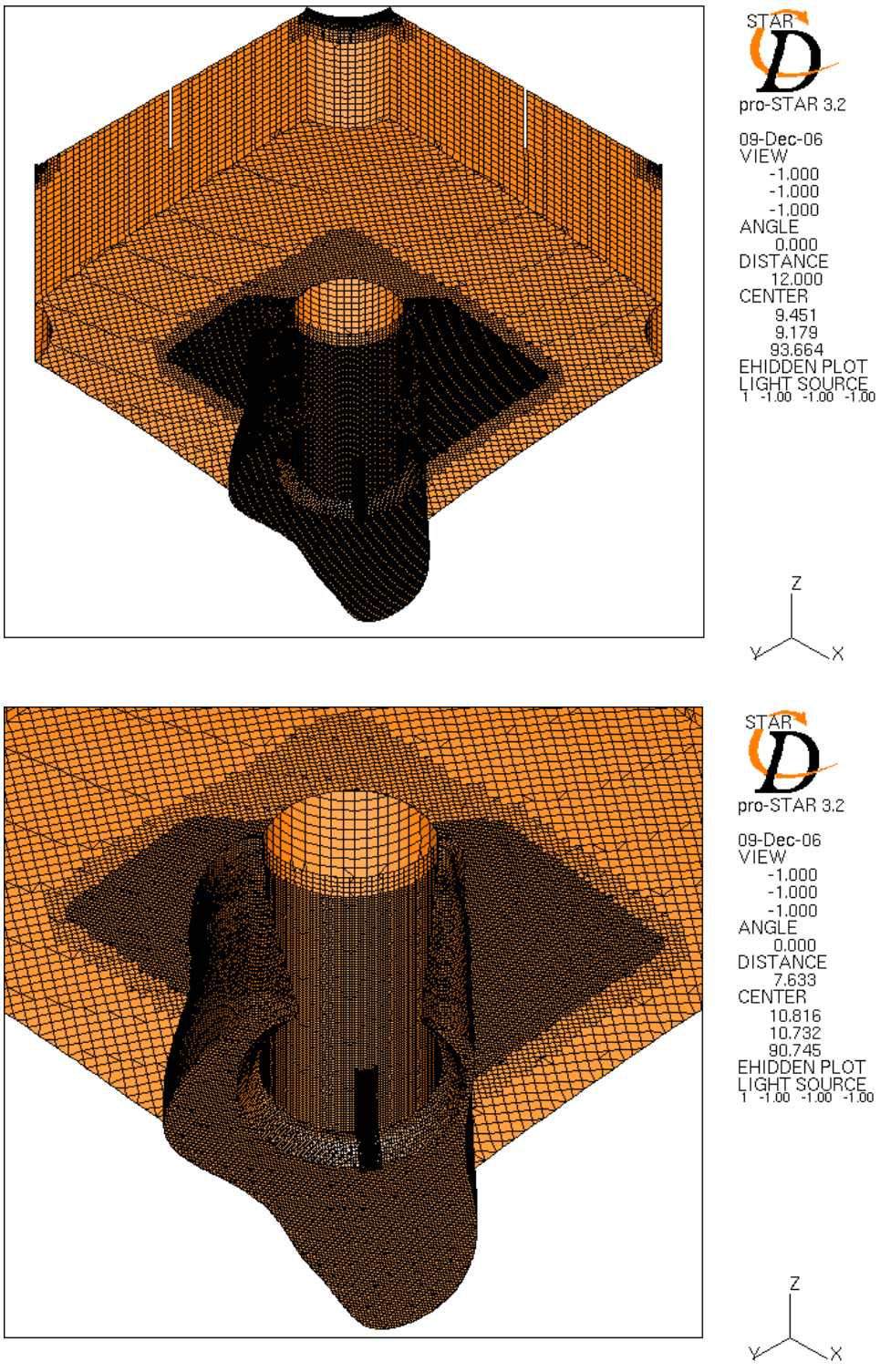

Figure 9.2(a) CFD Model Mesh for Case 4 Large Wastage Cavity

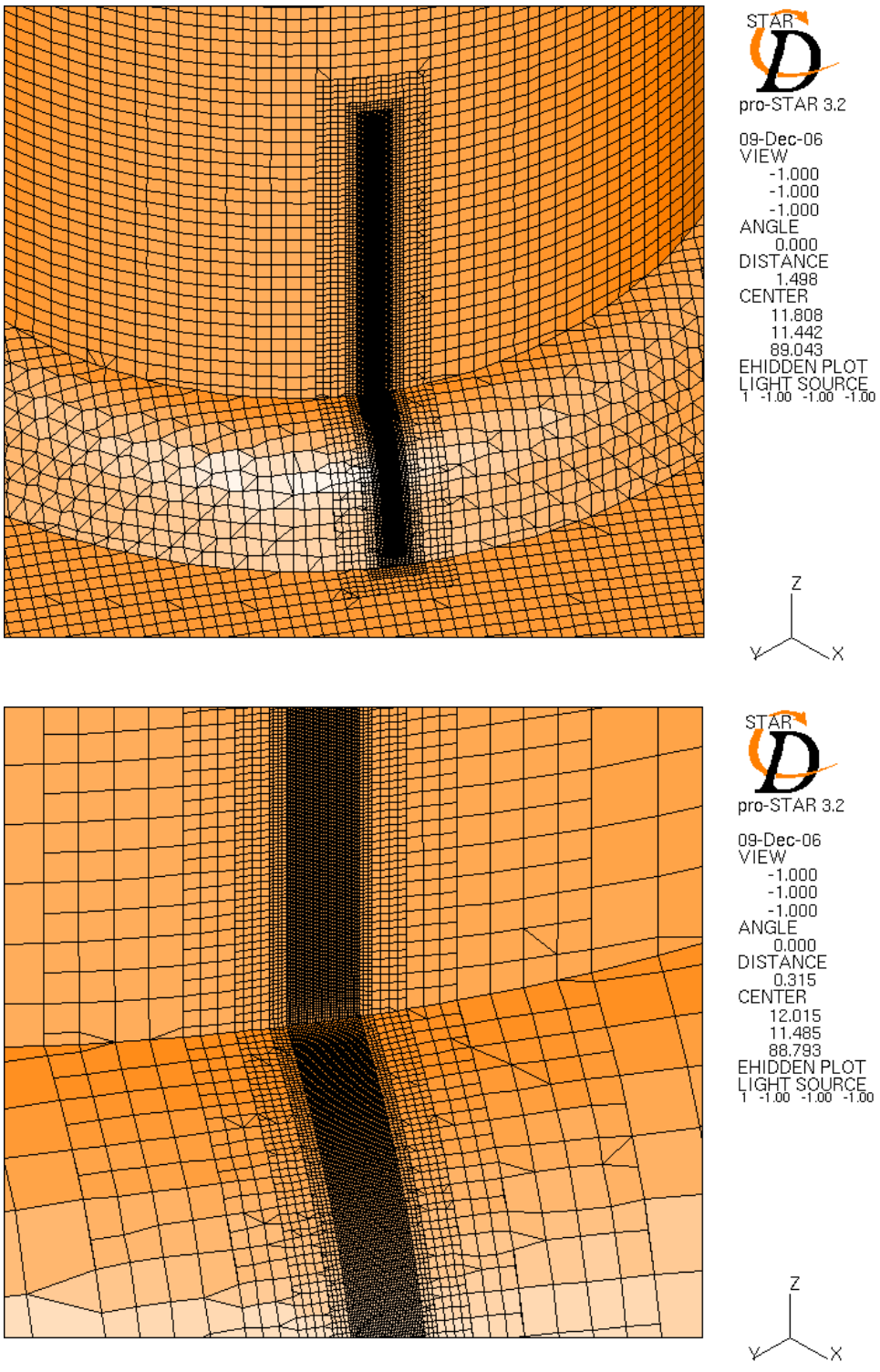

Figure 9.2(b) CFD Model Mesh for Case 4 Large Wastage Cavity

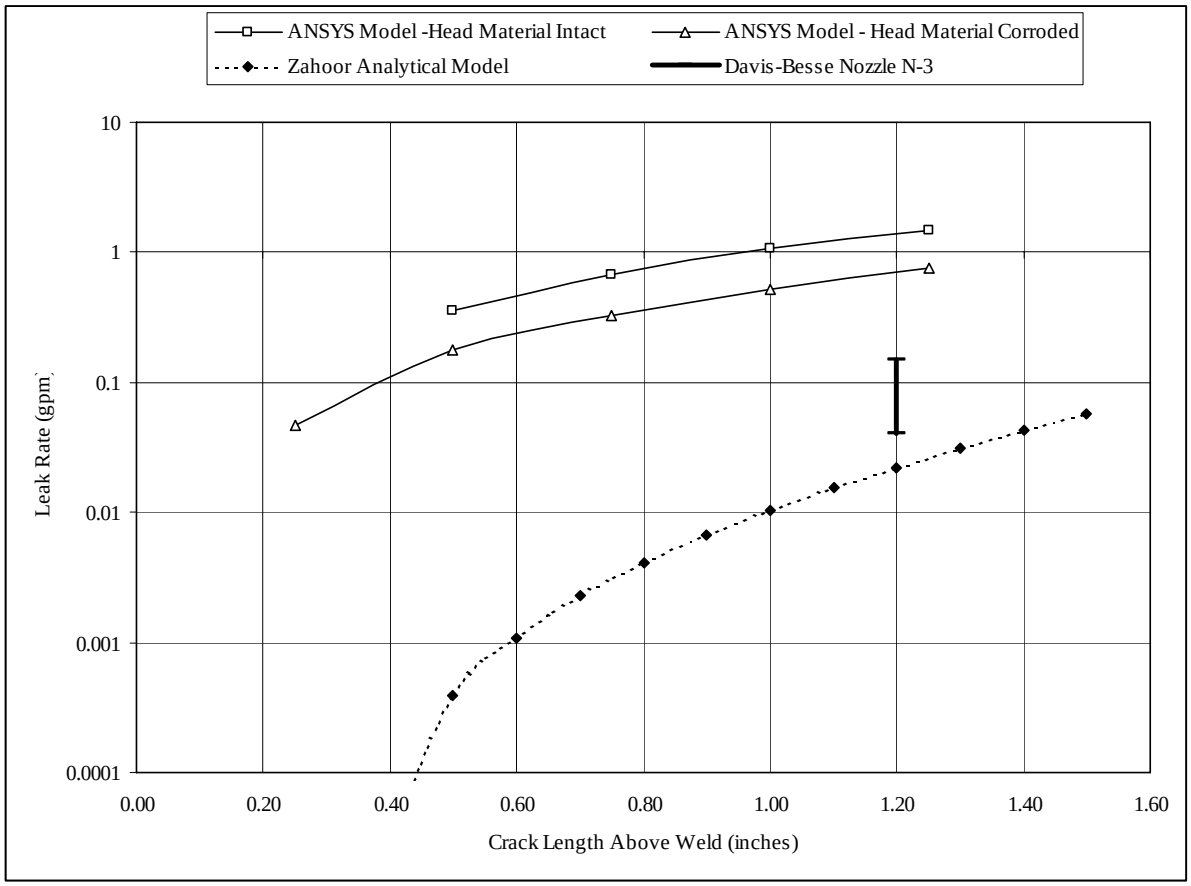

Figure 9.3 Calculated Leak Rate vs. Crack Length Above the J-Groove Weld as Calculated by Dominion Engineering, Inc.[1,2]

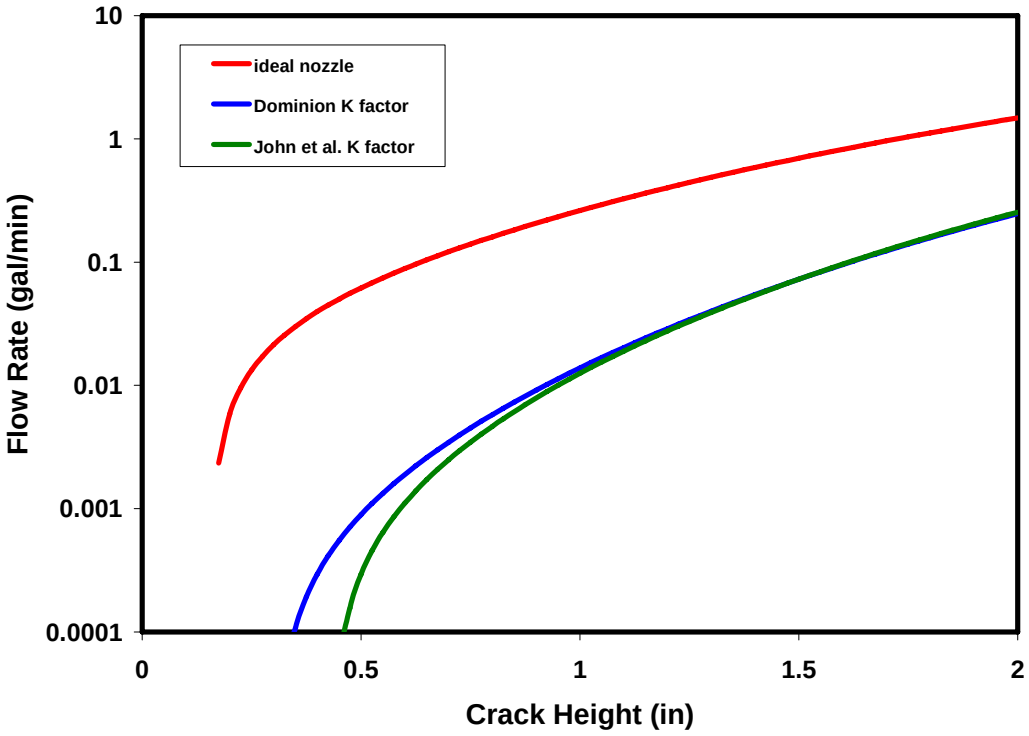

Figure 9.4 CRDM Nozzle Leak Rate vs. Crack Height.

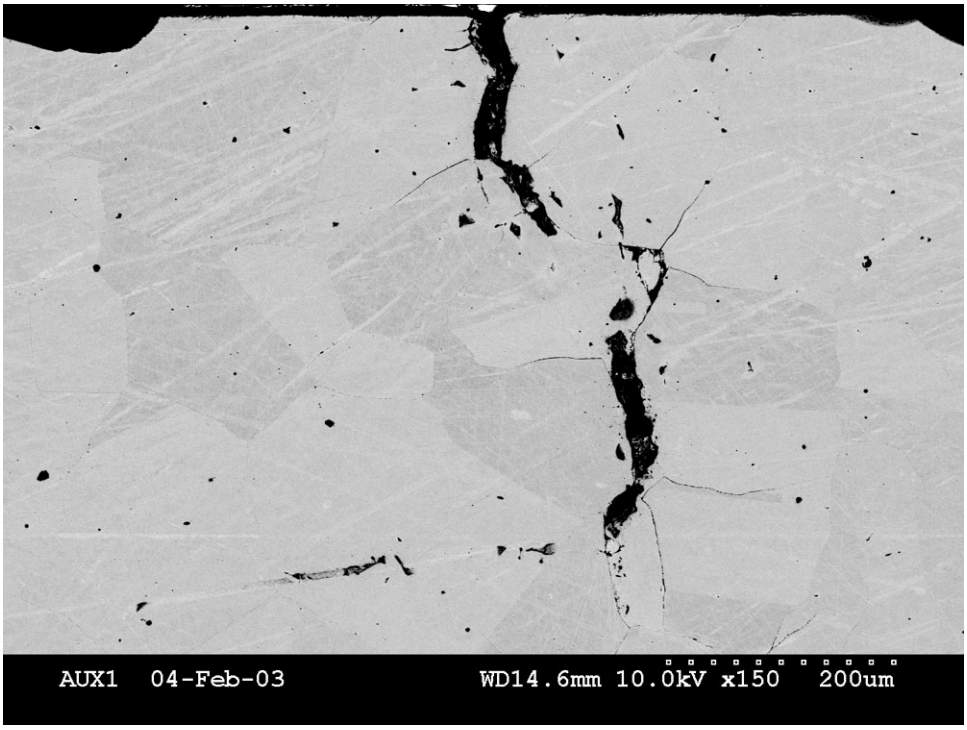

Figure 9.5 Scanning electron micrograph of CRDM Nozzle 3 crack at 180° location showing typical dimensions of PWSCC nozzle crack widths. Note the maximum crack width is about 20 μm (0.0008 inches). [10]

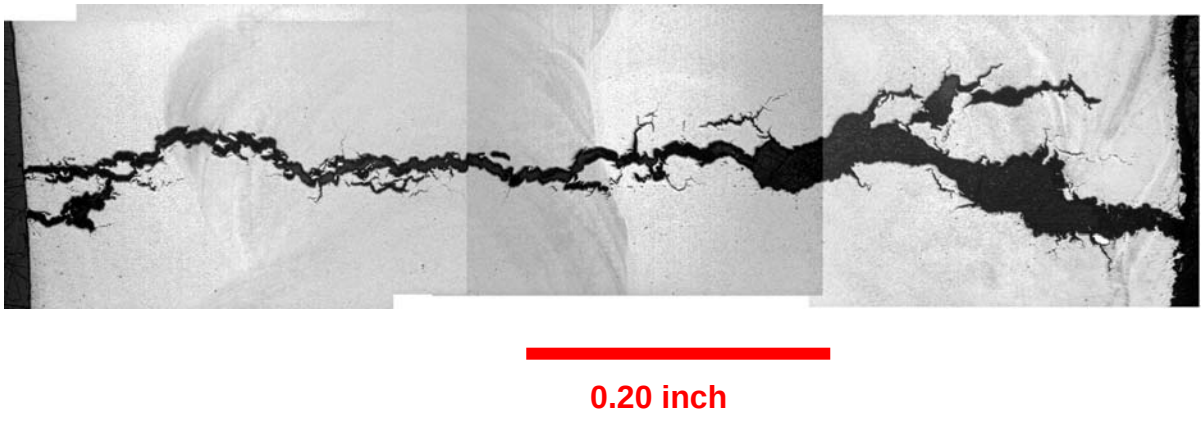

Figure 9.6 Optical micrograph of J-groove weld crack in CRDM Nozzle 3 at 10° location showing large crack width. Note the nominal crack width is about 400 μm (0.016 inches) or about 20 times larger than the PWSCC crack in the same nozzle shown above.[11]

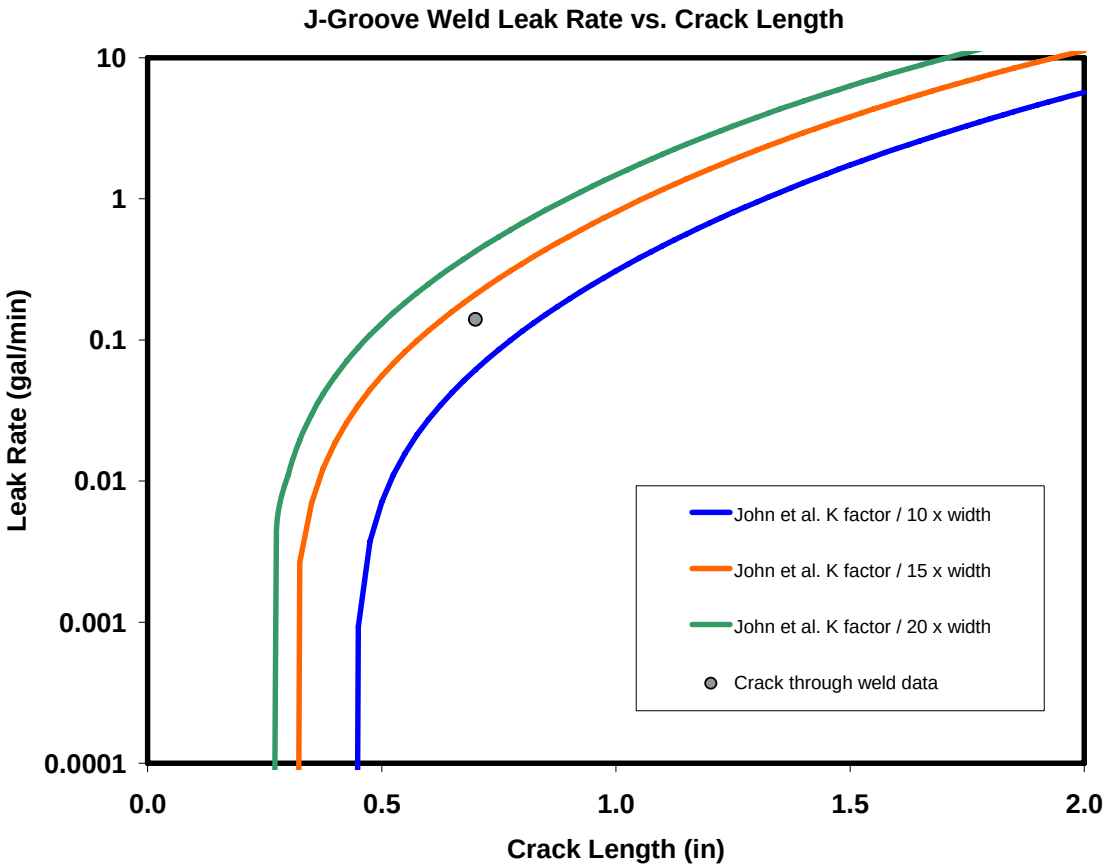

Figure 9.7 Calculated leak rate vs. crack length for a J-groove weld crack with crack widths that are 10 times, 15 times, and 20 times wider than typical PWSCC nozzle cracks.

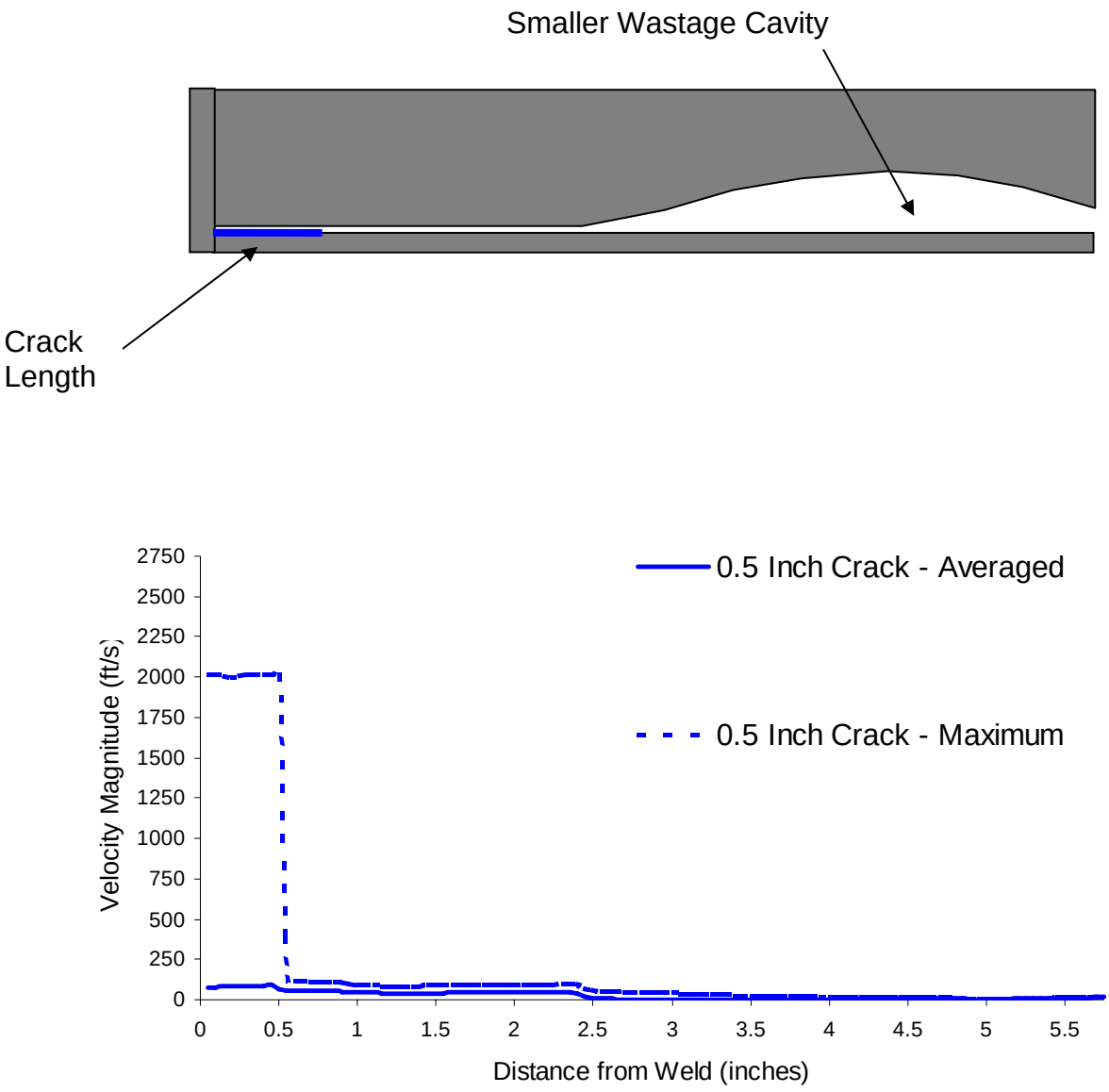

Figure 9.8 Case 1: Maximum and average fluid velocity magnitude within wastage as a function of distance to the J-groove weld for a 0.5-inch crack with a leak rate of 0.001 gpm.

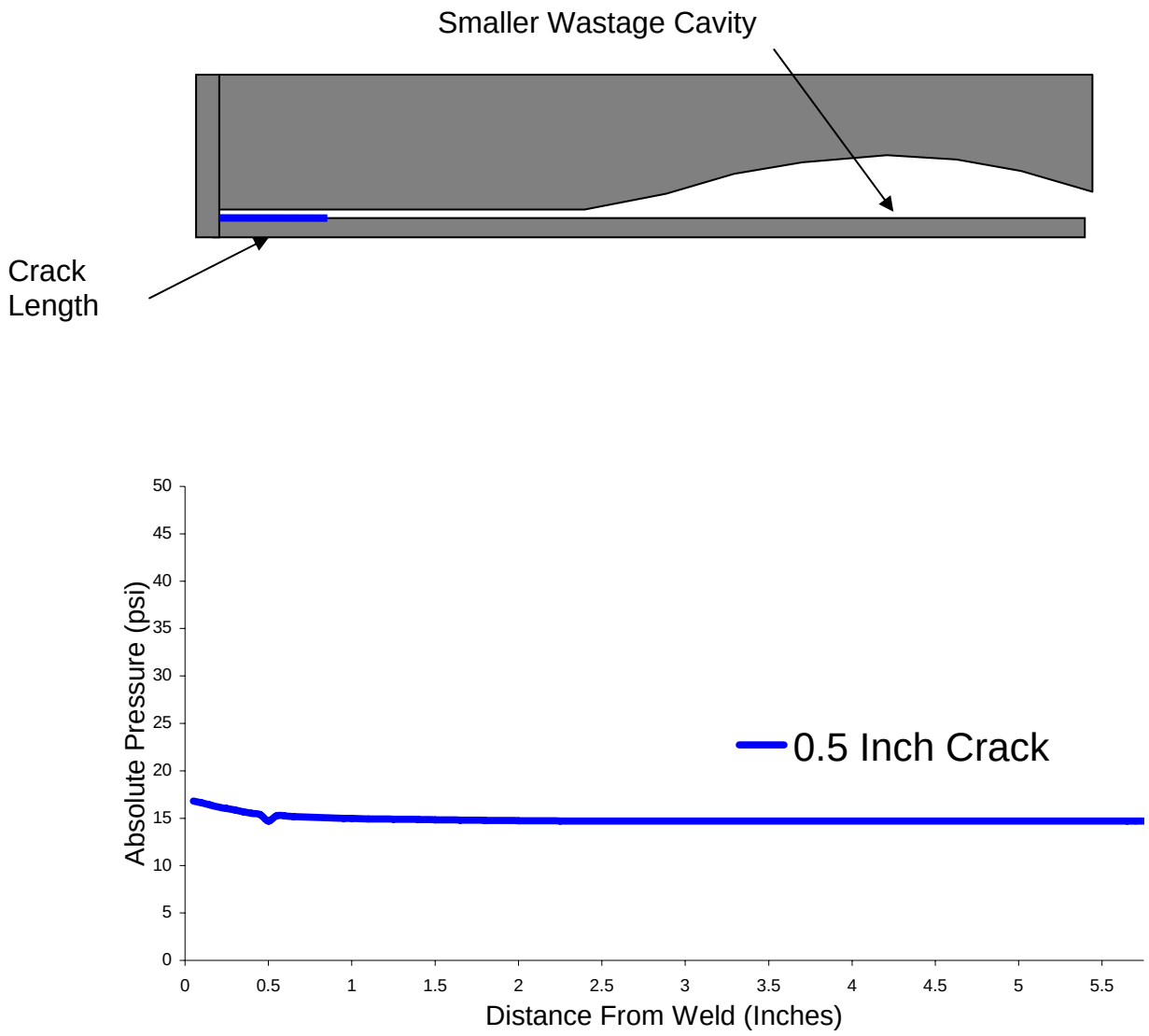

Figure 9.9 Case 1: Average fluid pressure within wastage as a function of distance to the J-groove weld for a 0.5-inch crack with a leak rate of 0.001 gpm.

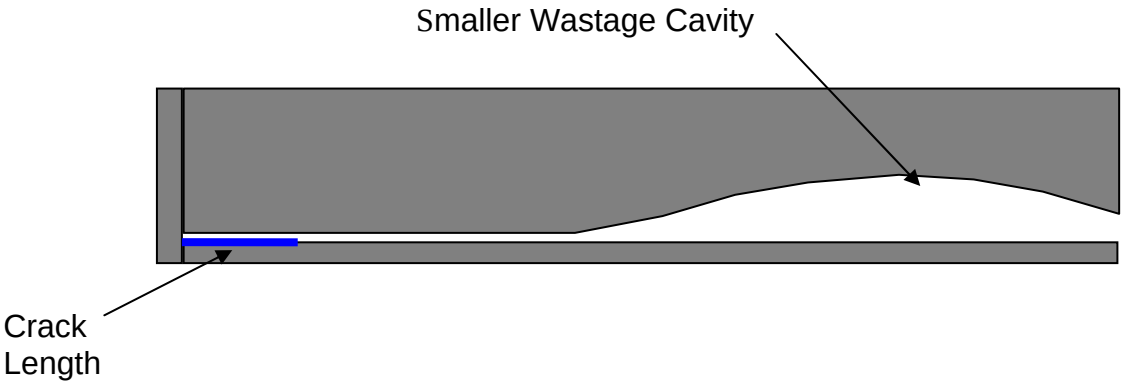

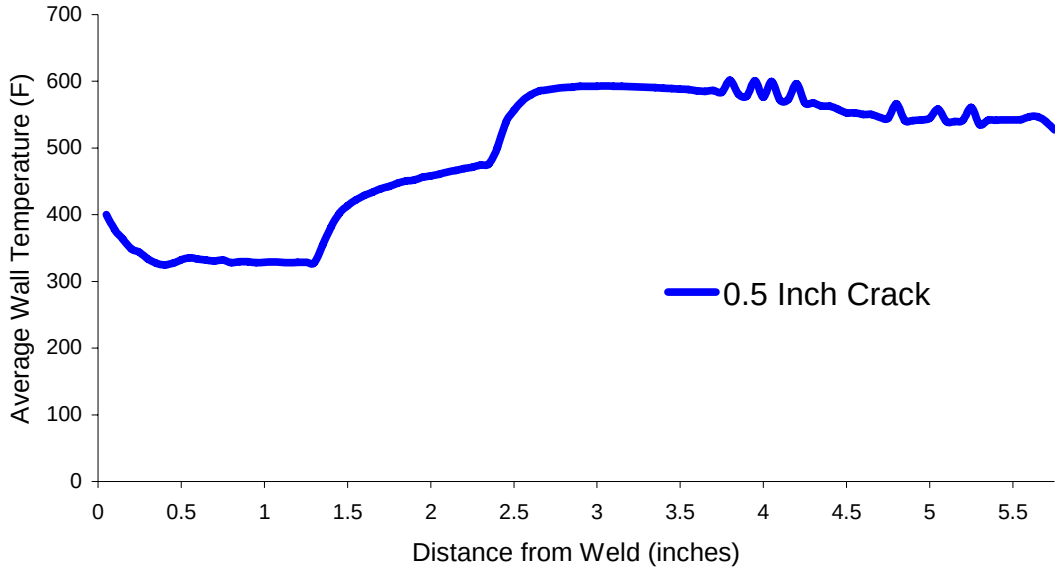

Figure 9.10 Case 1: Average wall temperature within wastage as a function of distance to the J-groove weld for a 0.5-inch crack with a leak rate of 0.001 gpm.

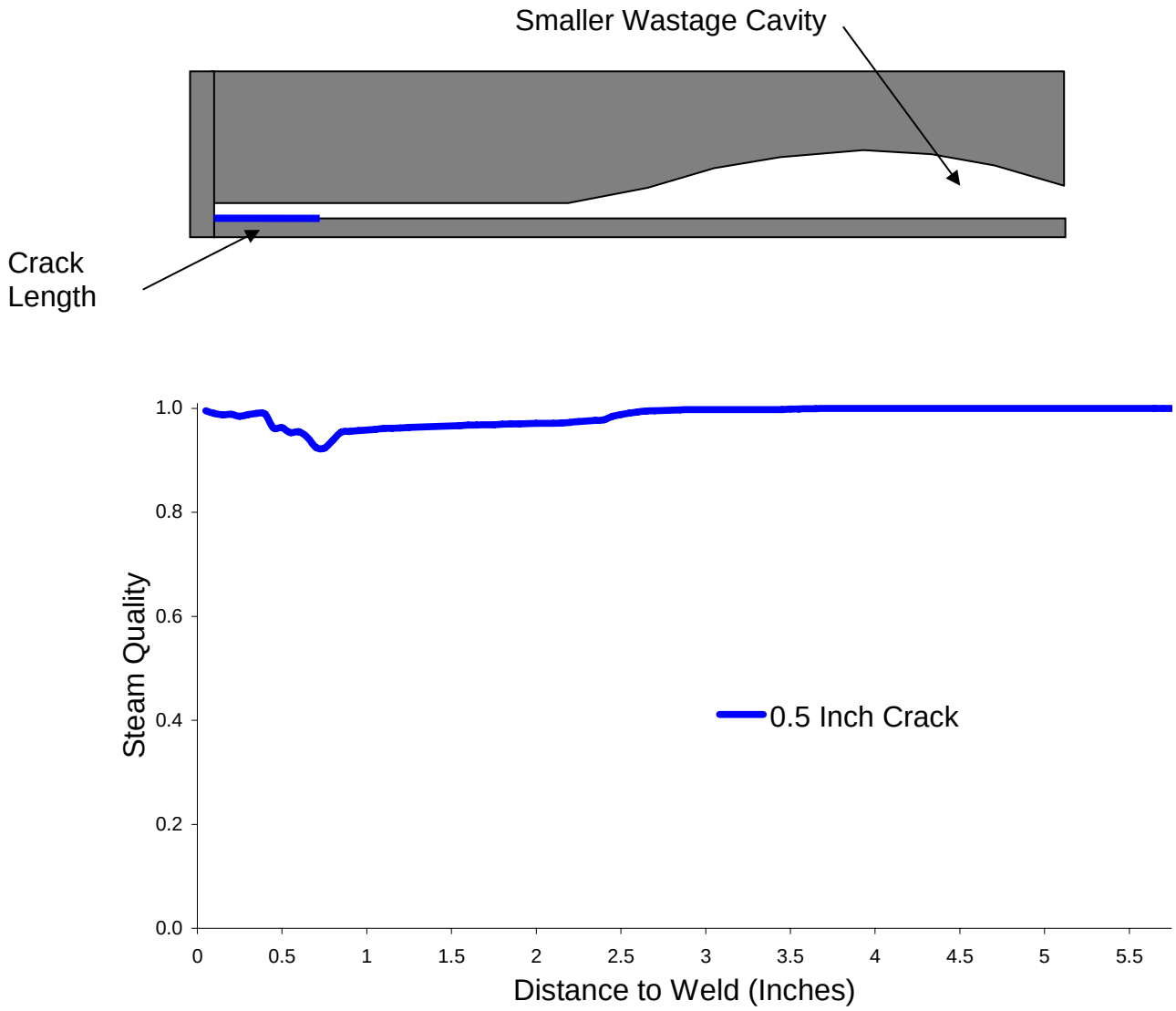

Figure 9.11 Case 1: Average steam quality within wastage as a function of distance to the J-groove weld for a 0.5-inch crack with a leak rate of 0.001 gpm.

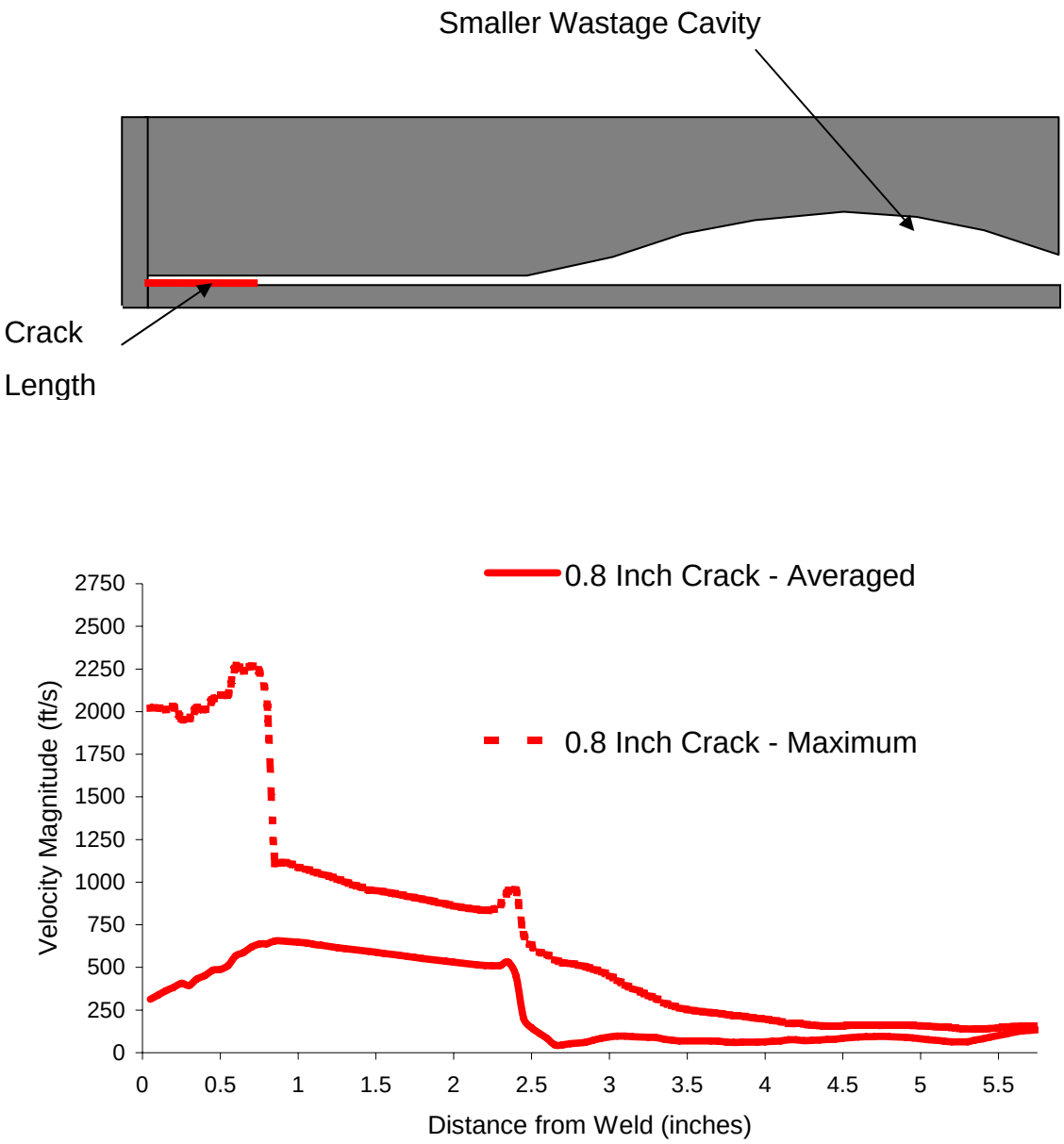

Figure 9.12 Case 2: Maximum and average fluid velocity magnitude within wastage as a function of distance from the J-groove weld for a 0.8-inch crack with a leak rate of 0.01 gpm.

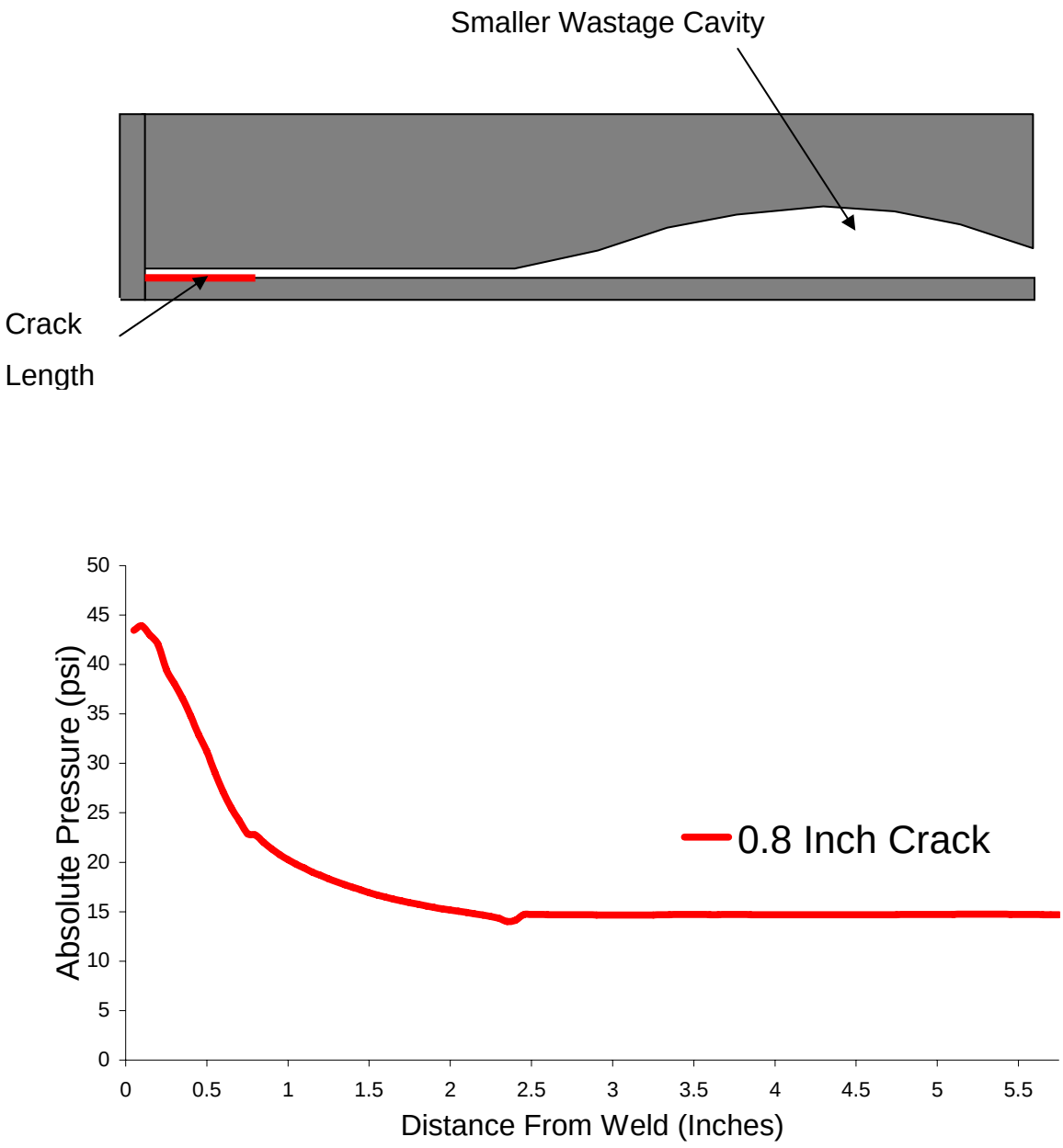

Figure 9.13 Case 2: Average fluid pressure within wastage as a function of distance to the J-groove weld for a 0.8-inch crack with a leak rate of 0.01 gpm.

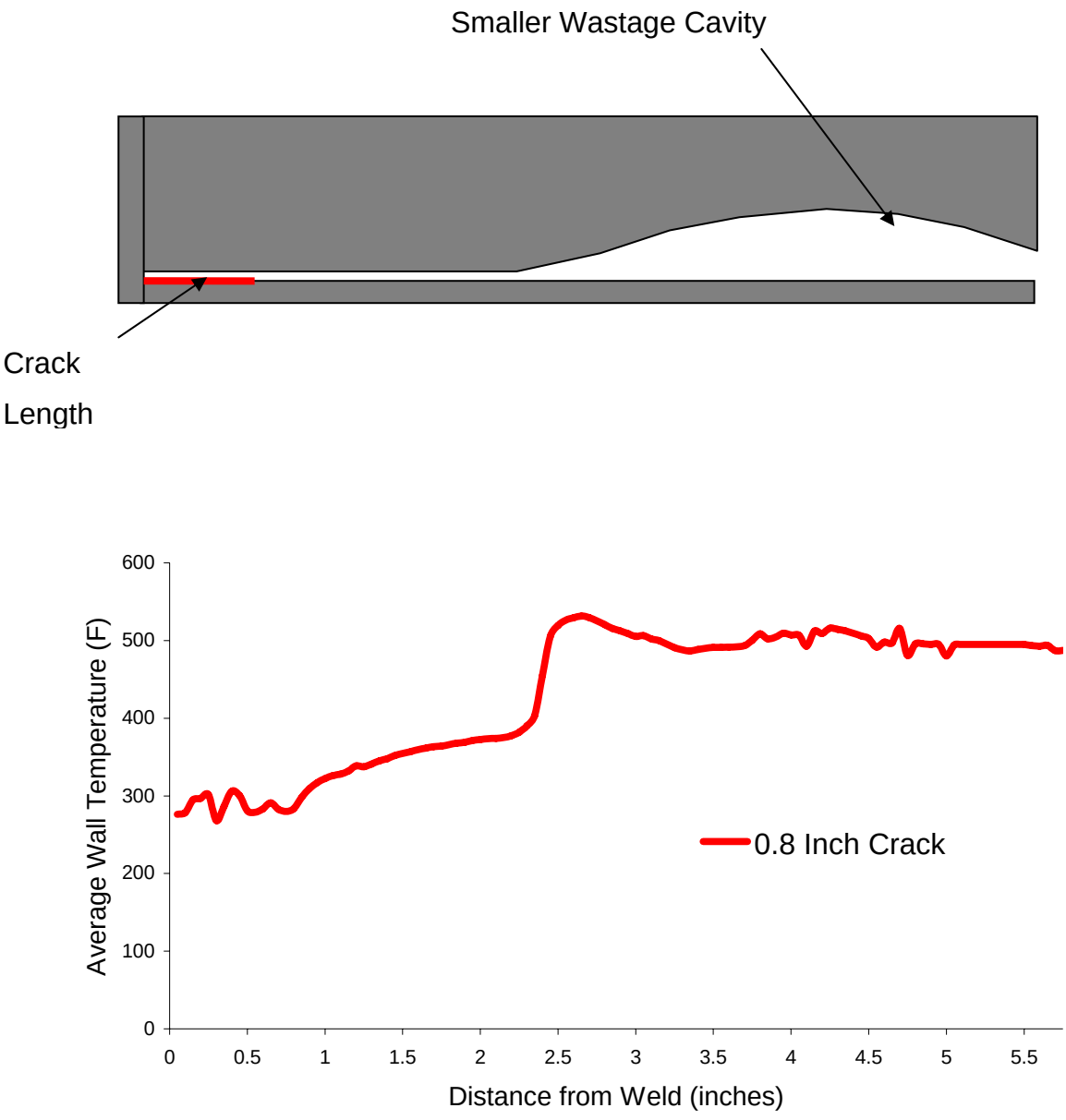

Figure 9.14 Case 2: Average wall temperature within wastage as a function of distance to the J-groove weld for a 0.8-inch crack with a leak rate of 0.01 gpm.

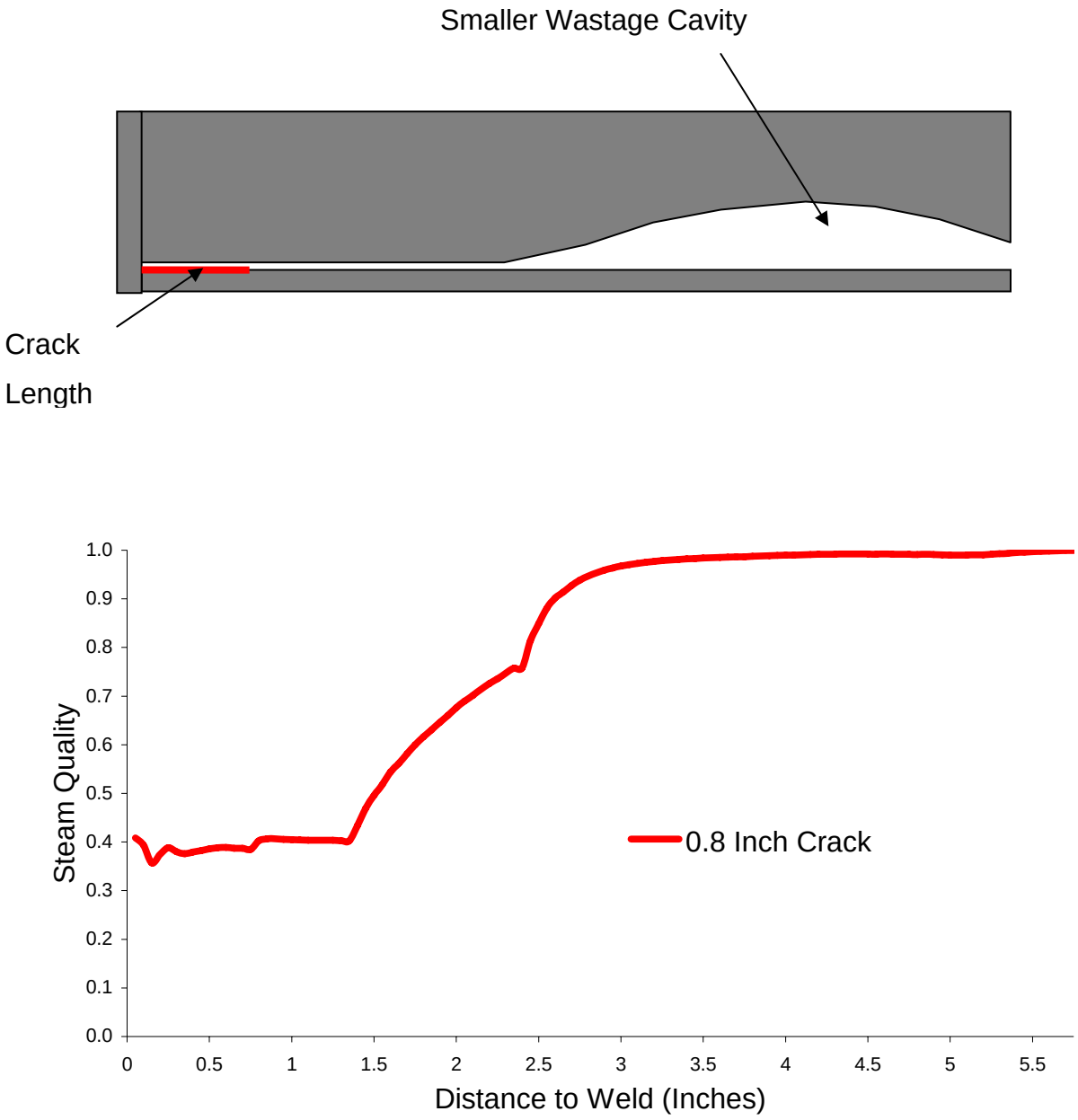

Figure 9.15 Case 2: Average steam quality within wastage as a function of distance to the J-groove weld for a 0.8-inch crack with a leak rate of 0.01 gpm.

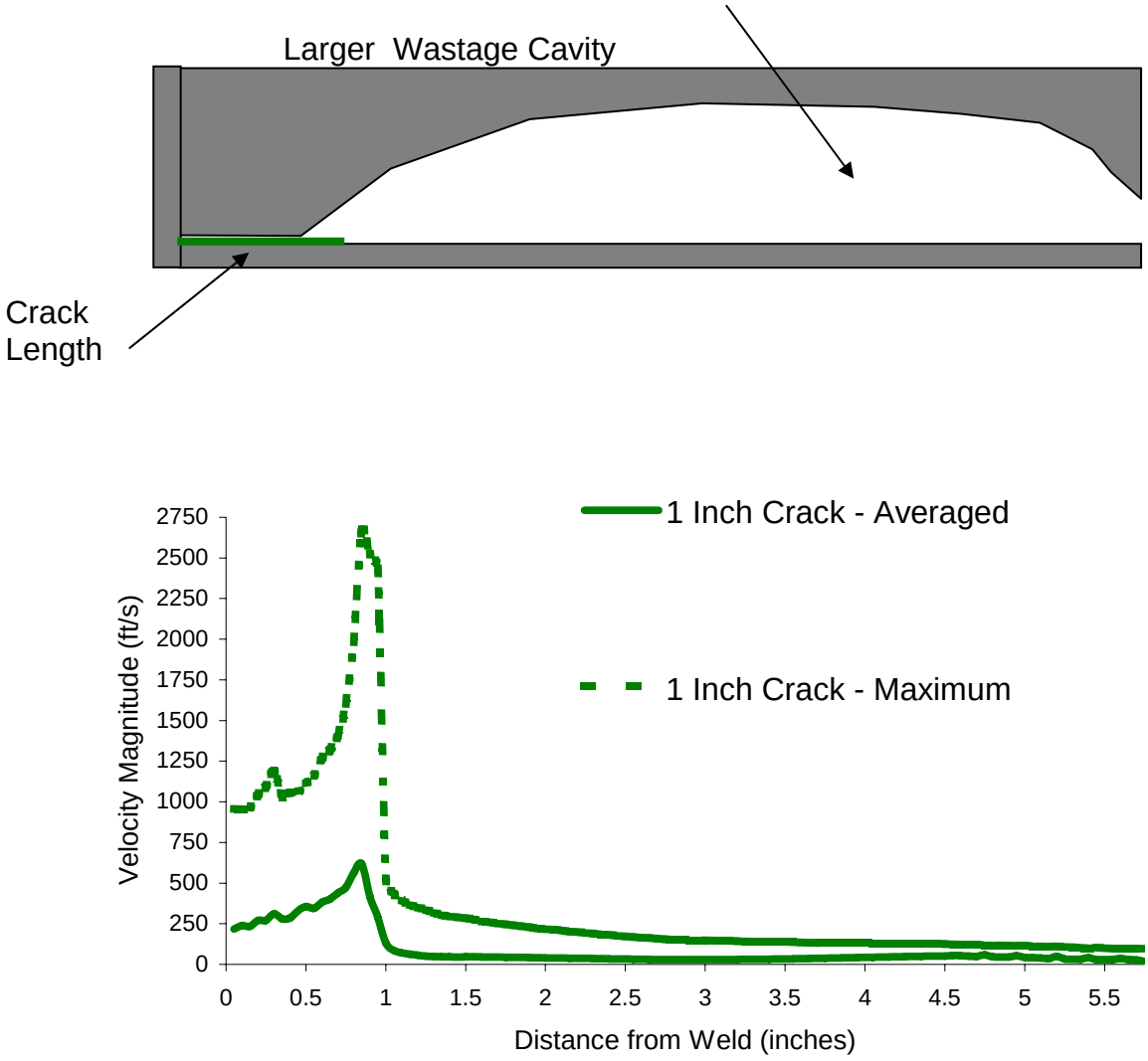

Figure 9.16 Case 3: Maximum and average fluid velocity magnitude within wastage as a function of distance to the J-groove weld for a 1.0-inch crack with a leak rate of 0.02 gpm.

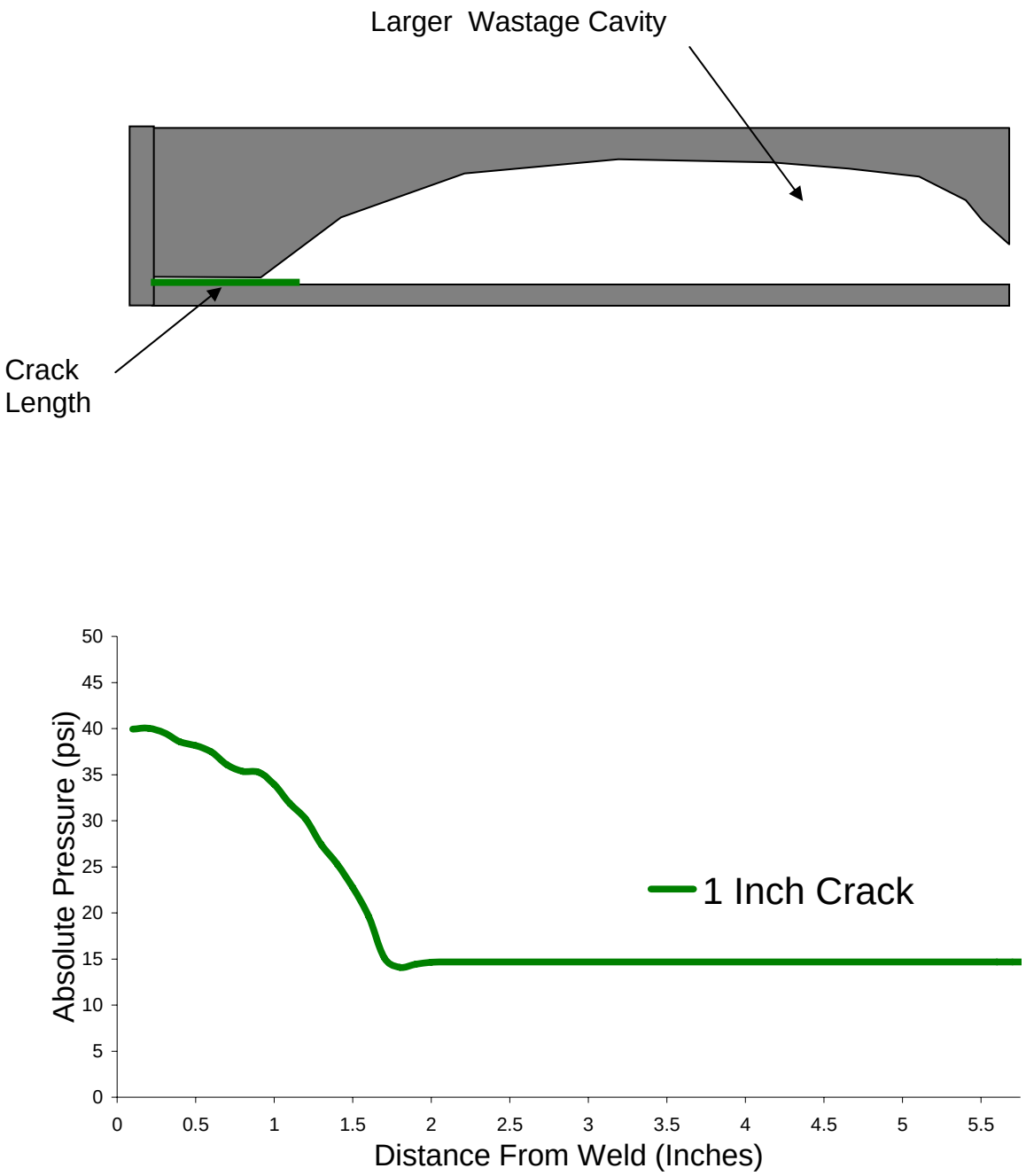

Figure 9.17 Case 3: Average fluid pressure within wastage as a function of distance to the J-groove weld for a 1.0-inch crack with a leak rate of 0.02 gpm.

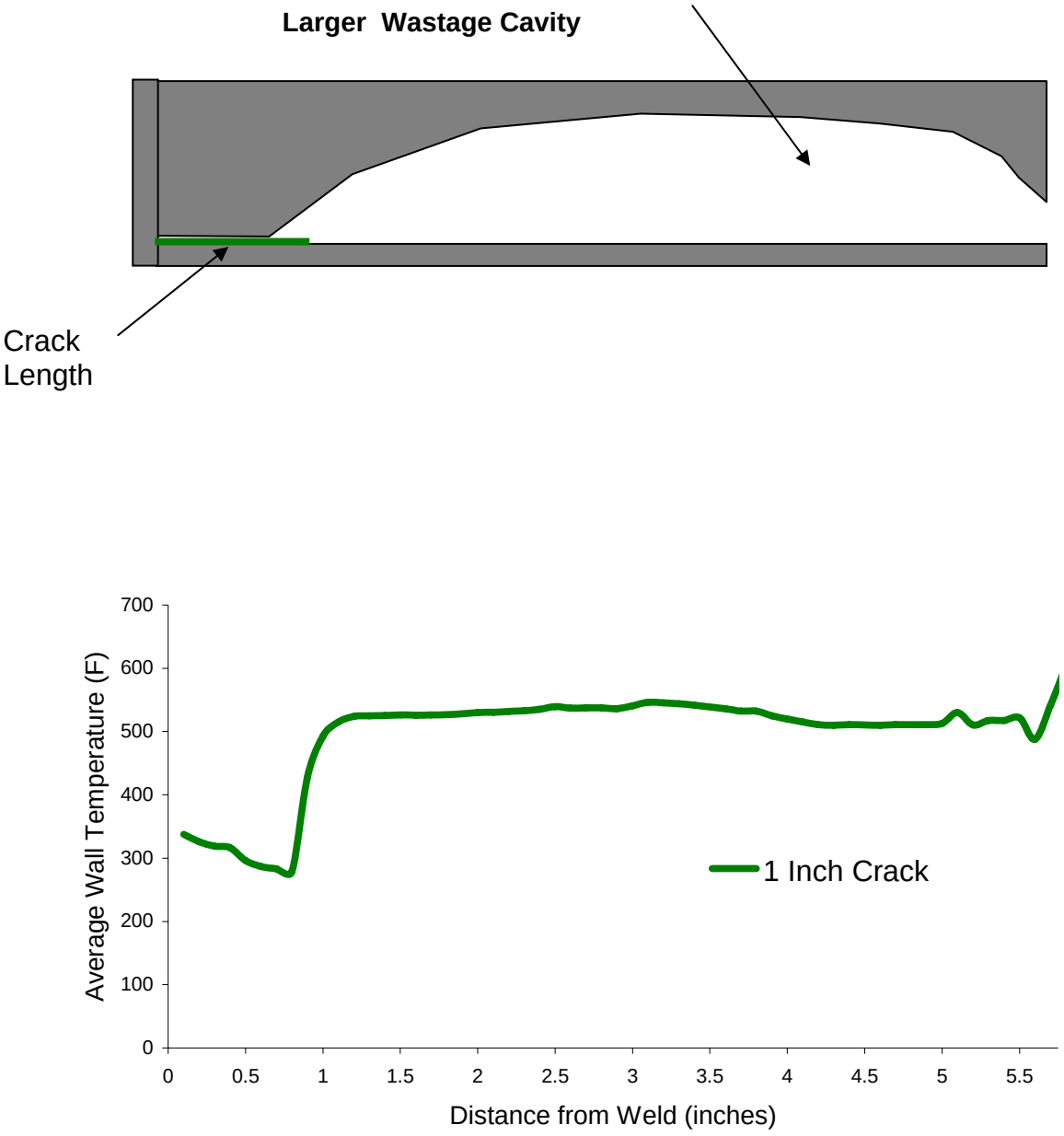

Figure 9.18 Case 3: Average temperature within wastage as a function of distance to the J-groove weld for a 1.0-inch crack with a leak rate of 0.02 gpm.

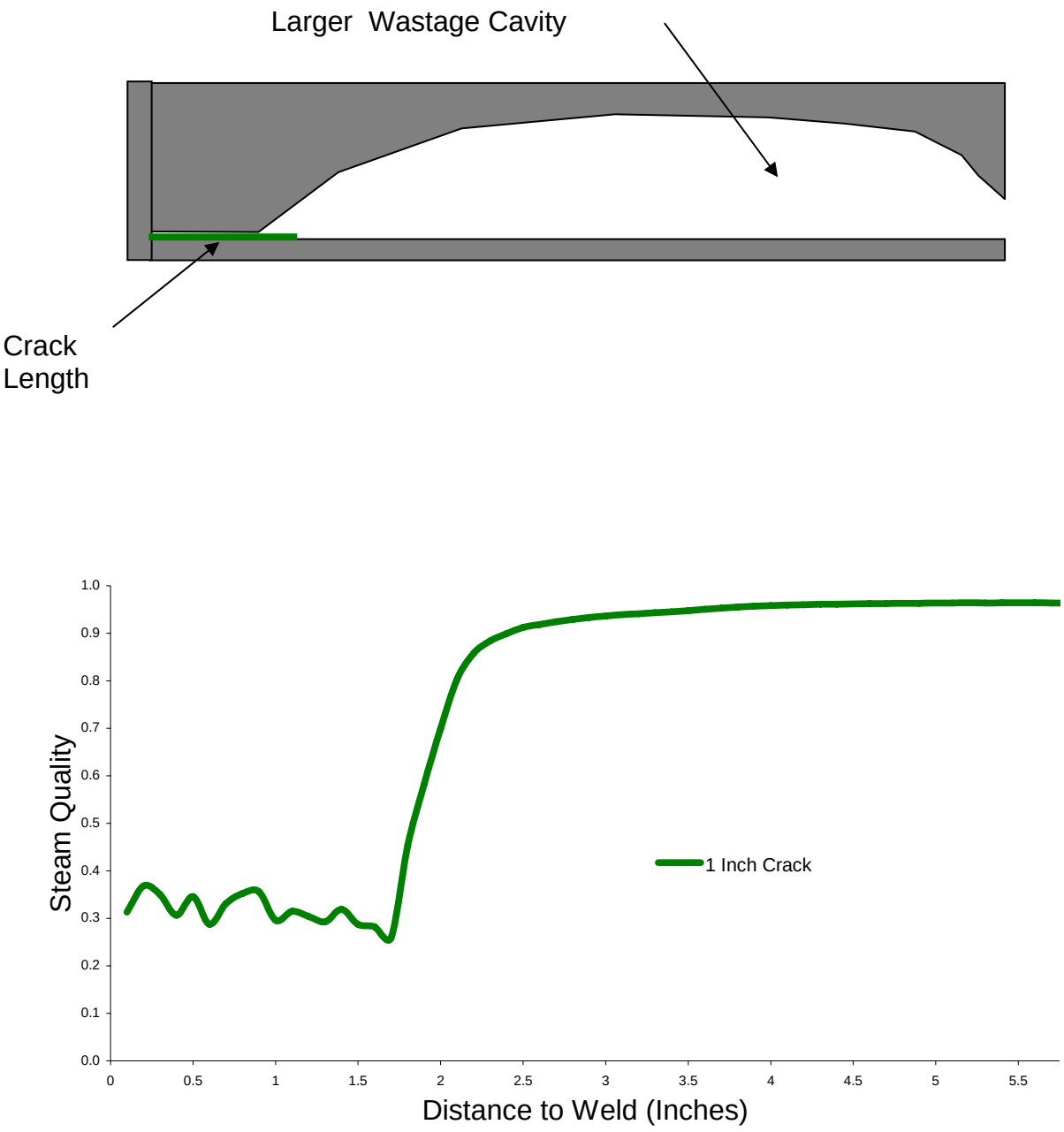

Figure 9.19 Case 3: Average steam quality within wastage as a function of distance to the J-groove weld for a 1.0-inch crack with a leak rate of 0.02 gpm.

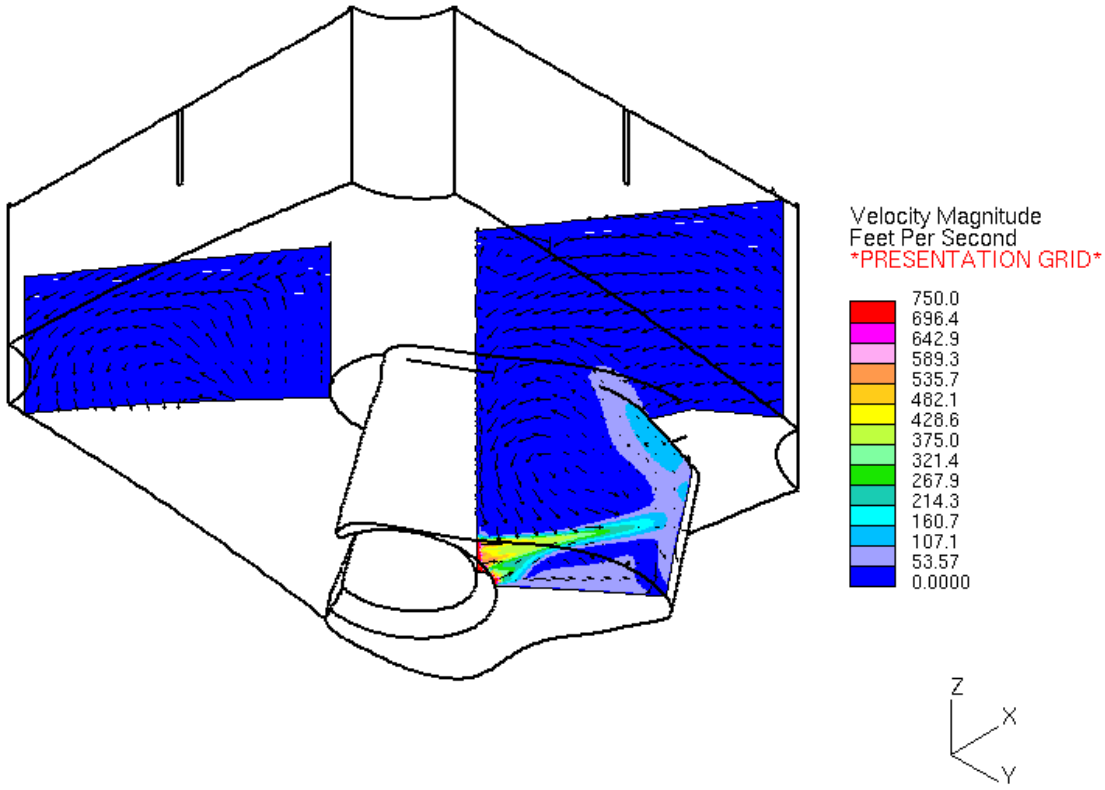

Figure 9.20 Velocity magnitude contours for the final wastage state sectioned directly through crack. The viewpoint is looking up from below RPV head.

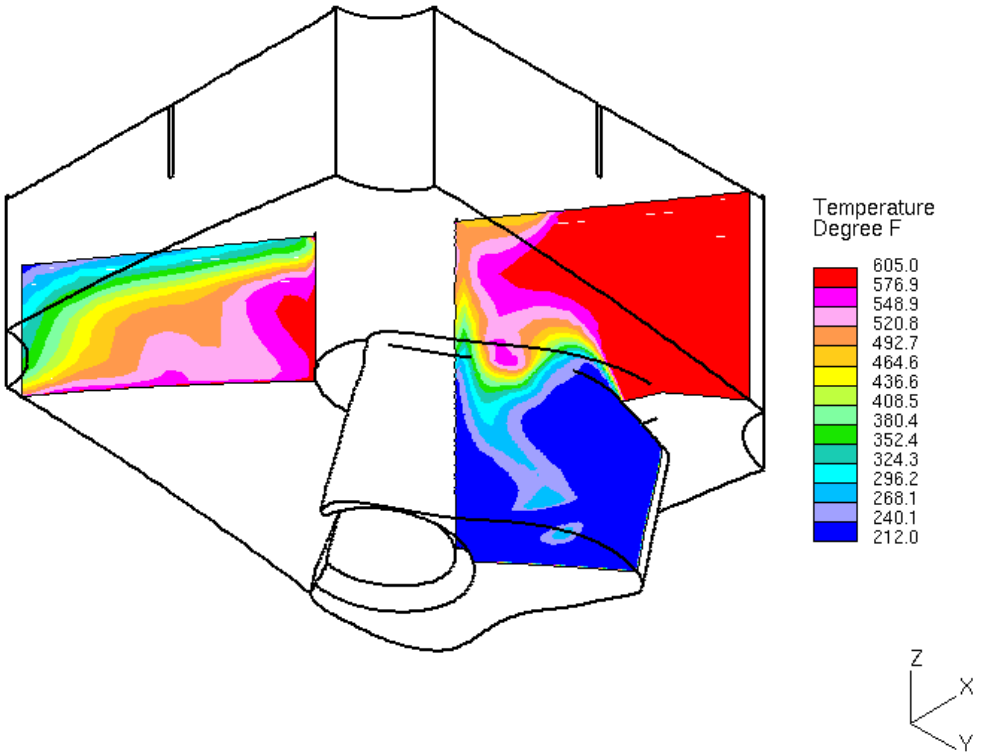

Figure 9.21 Temperature contours for the final wastage state sectioned directly through crack. The viewpoint is looking up from below RPV head.

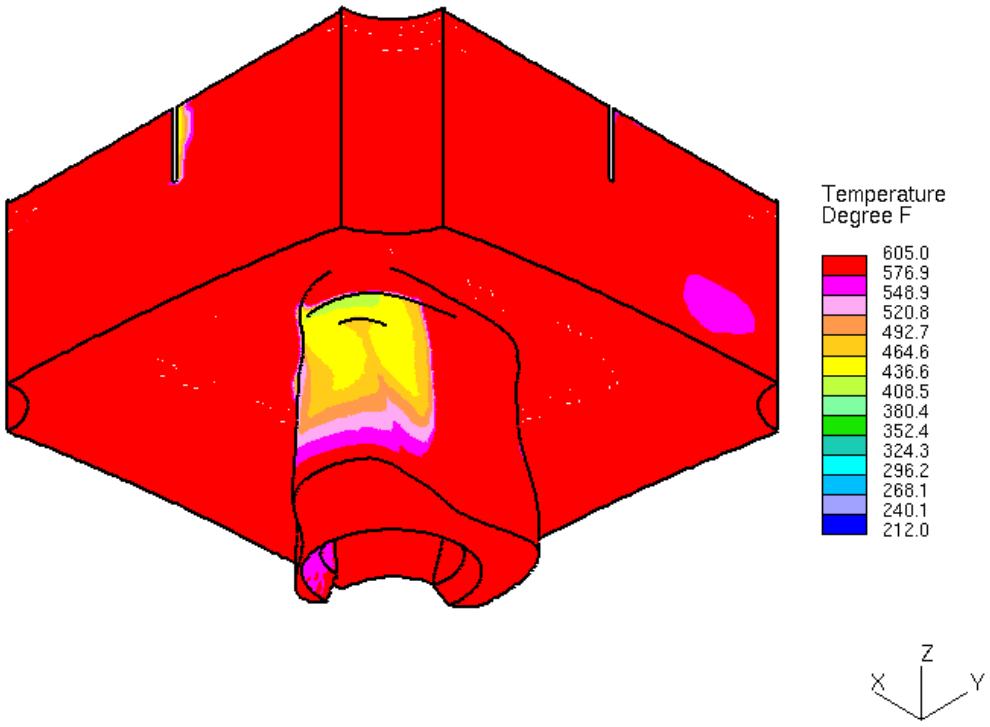

Figure 9.22 Cavity wall temperature contours for the final wastage state. The viewpoint is looking up from below RPV head from a different orientation than Figures 9.17 and 9.18 to show the cavity wall temperatures directly opposite the cracks.

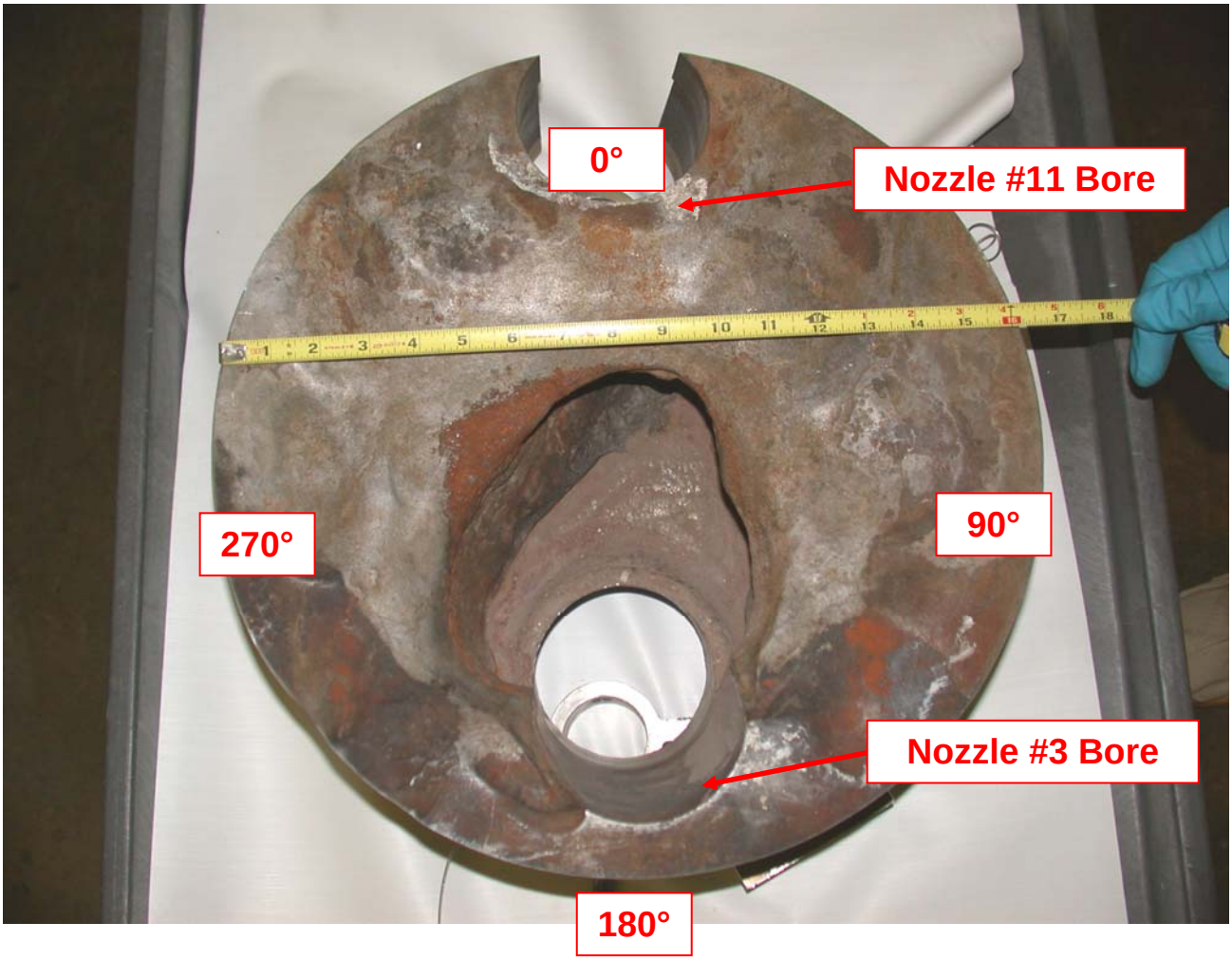

Figure 9.23 Top View of Wastage Cavity on Davis-Besse RPV Head.[13]

Looking toward 90° ~0.7X

Looking toward 270° ~0.5X

Figure 9.24 Wastage Cavity Sidewalls Viewed at Low Magnification Looking Toward 90º and 270º.[14]

Figure 9.25(a) Dental Mold of Wastage Cavity Looking Towards 0º and 90º.[15]

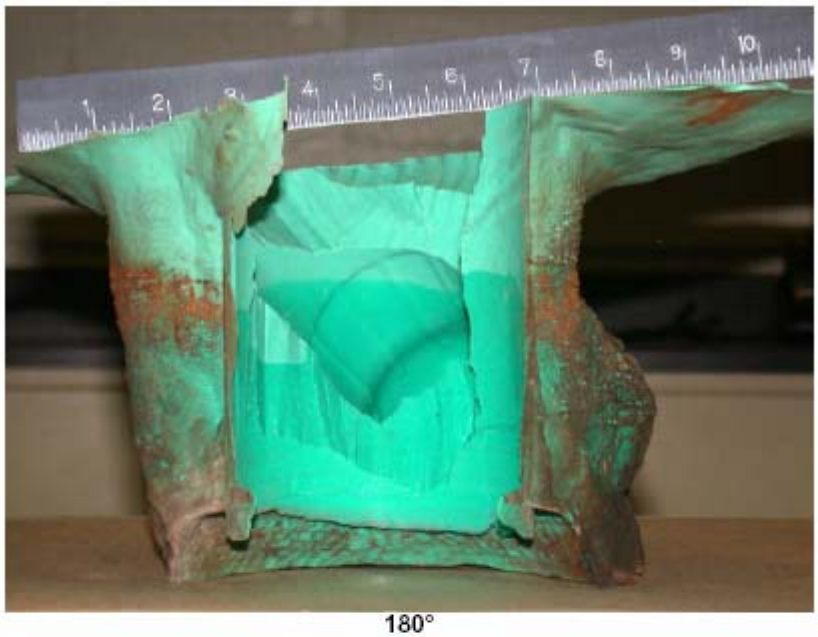

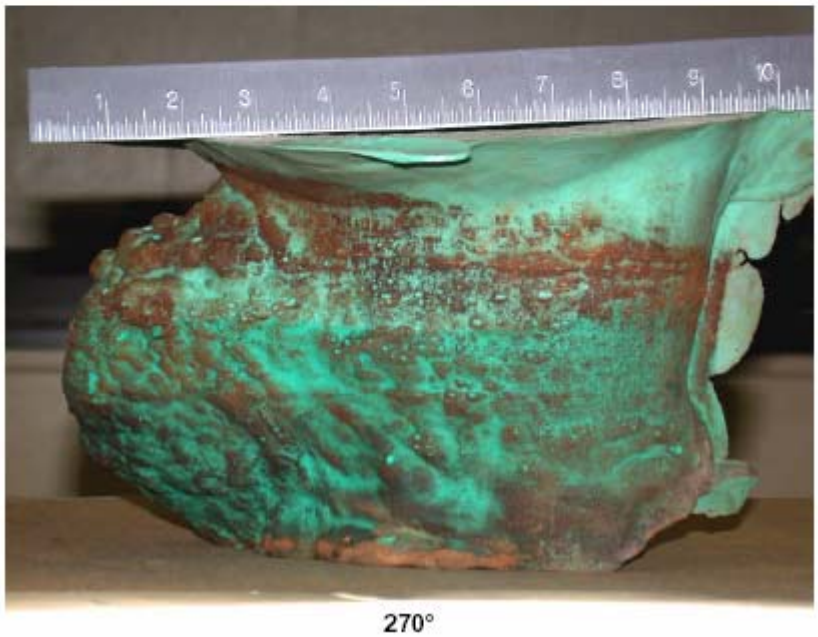

Figure 9.25(b) Dental Mold of Wastage Cavity Looking Towards 180º and 270º.[16]

(a) Top View Time – 0.001 seconds Perspective View

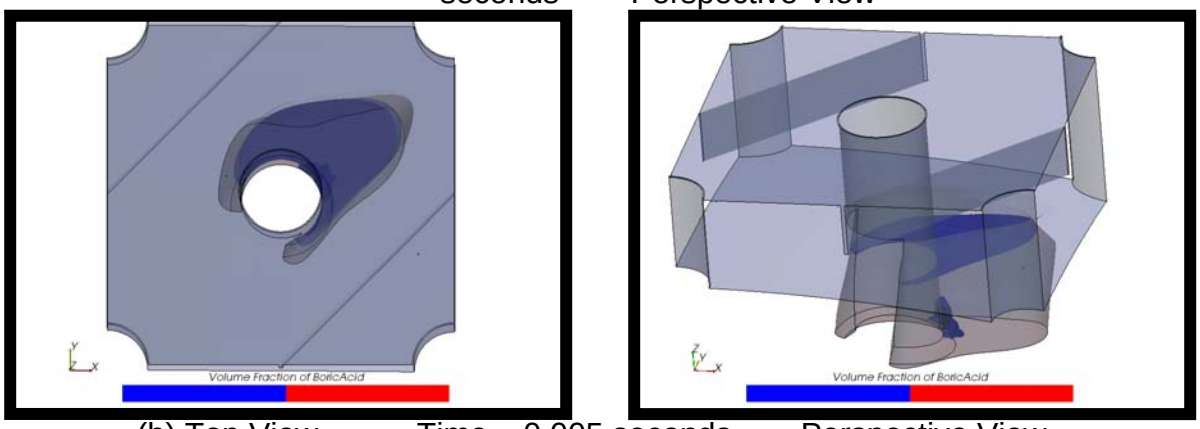

(b) Top View Time – 0.005 seconds Perspective View

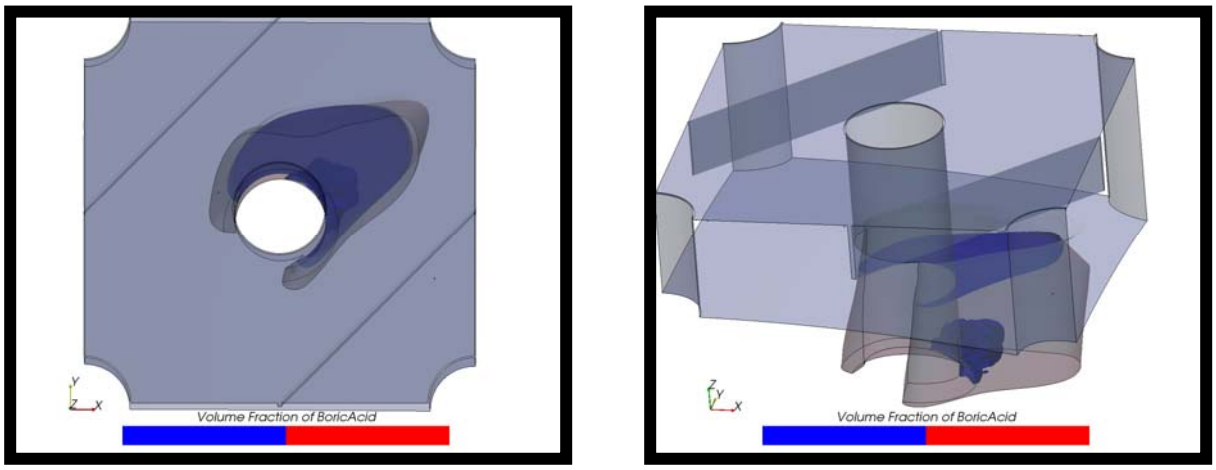

(c) Top View Time – 0.02 seconds Perspective View

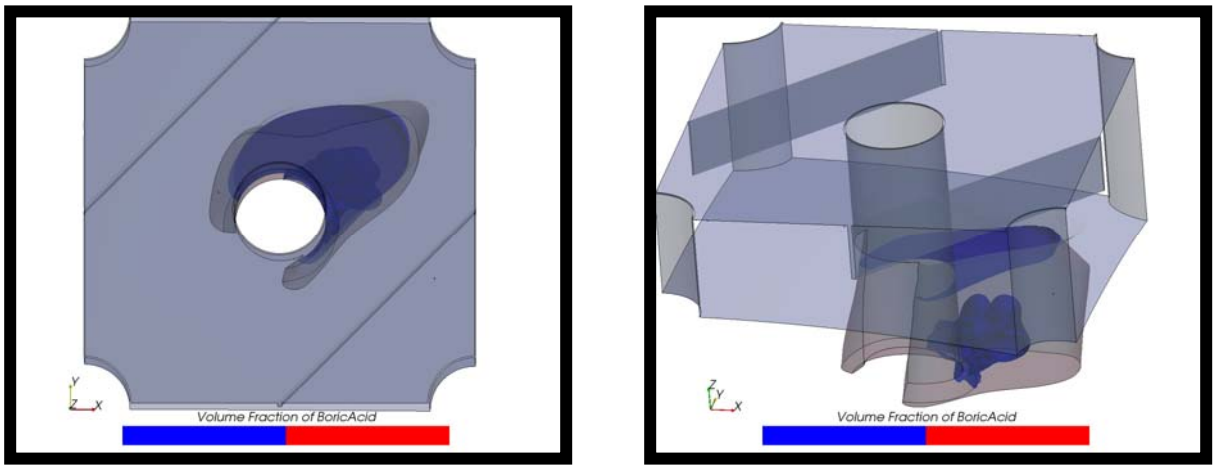

Figure 9.26 Transient analysis results for final wastage cavity filled with boric acid solution for time steps from 0.001 seconds to 0.02 seconds.

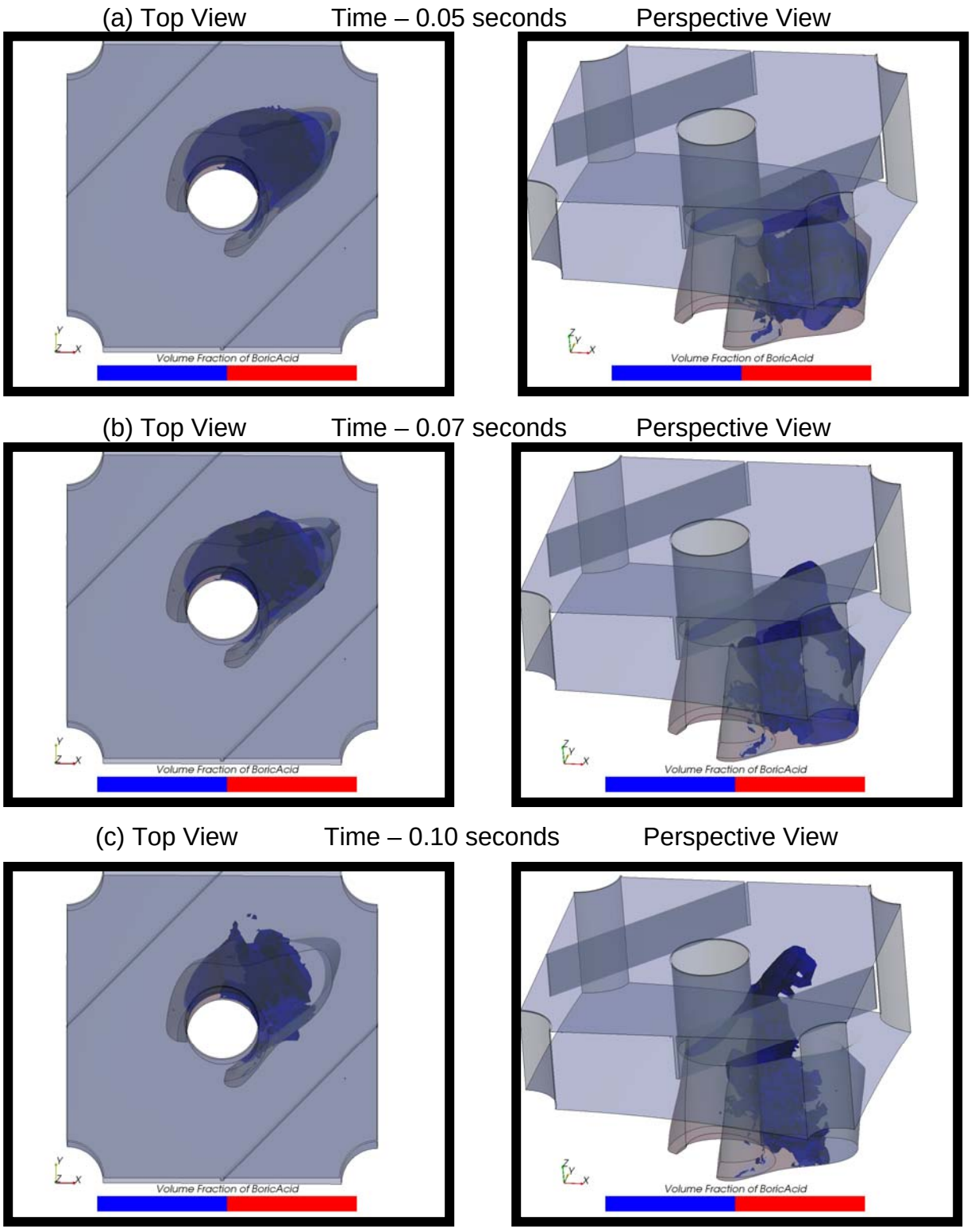

Figure 9.27 Transient analysis results for final wastage cavity filled with boric acid solution for time steps from 0.05 seconds to 0.10 seconds.

(a) Top View Time – 0.12 seconds Perspective View

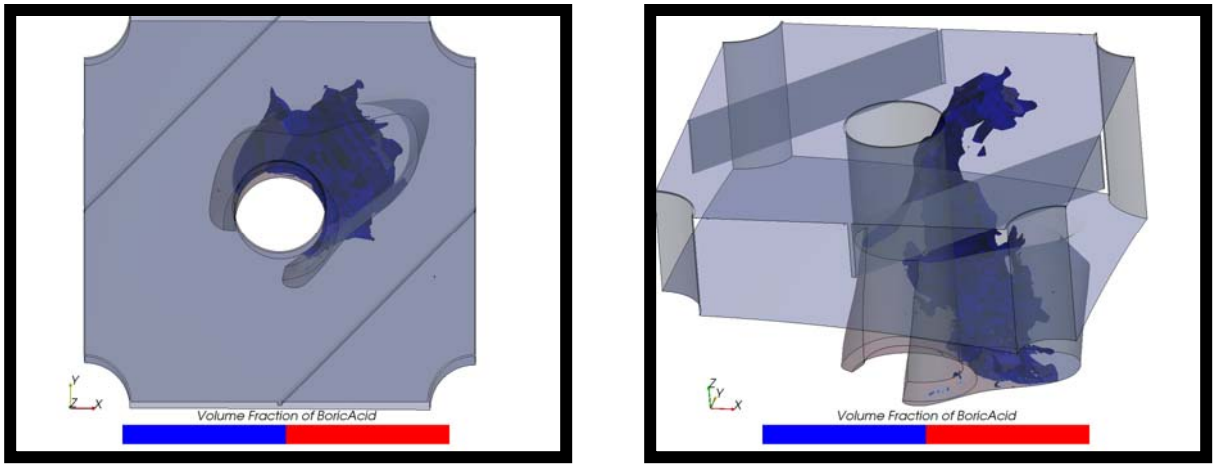

(b) Top View Time – 0.15 seconds Perspective View

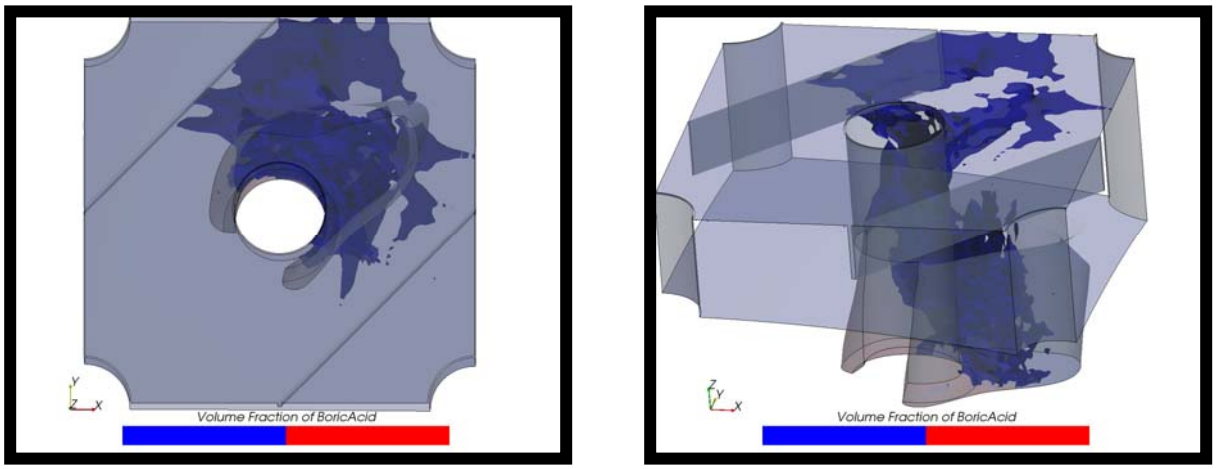

(c) Top View Time – 0.20 seconds Perspective View

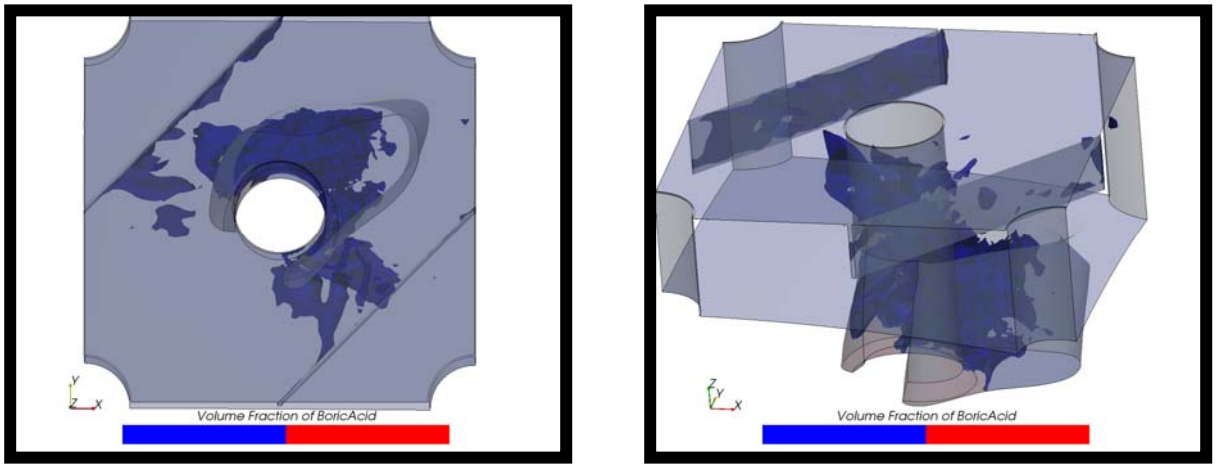

Figure 9.28 Transient analysis results for final wastage cavity filled with boric acid solution for time steps from 0.12 seconds to 0.20 seconds.

(a) Top View Time – 0.25 seconds Perspective View

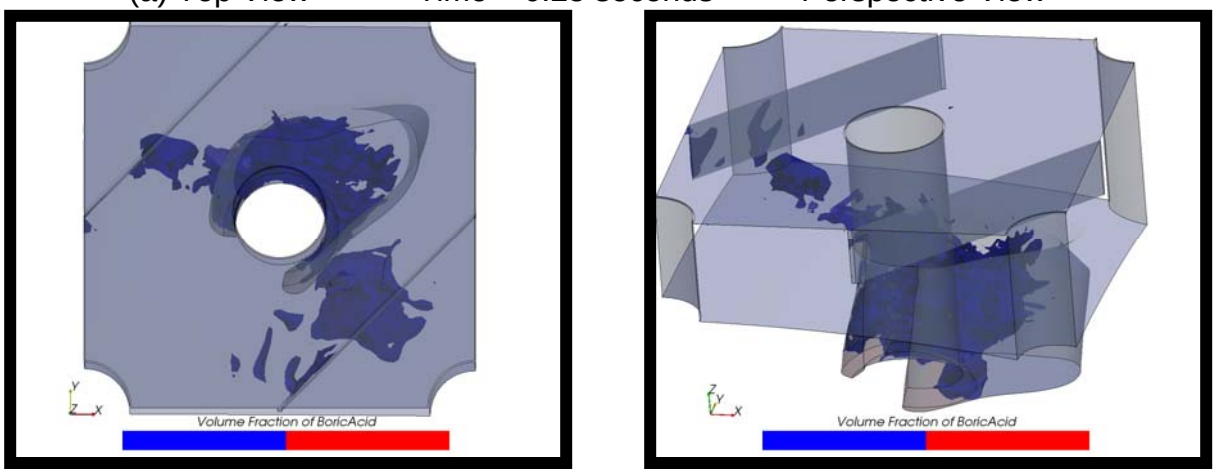

(b) Top View Time – 0.32 seconds Perspective View

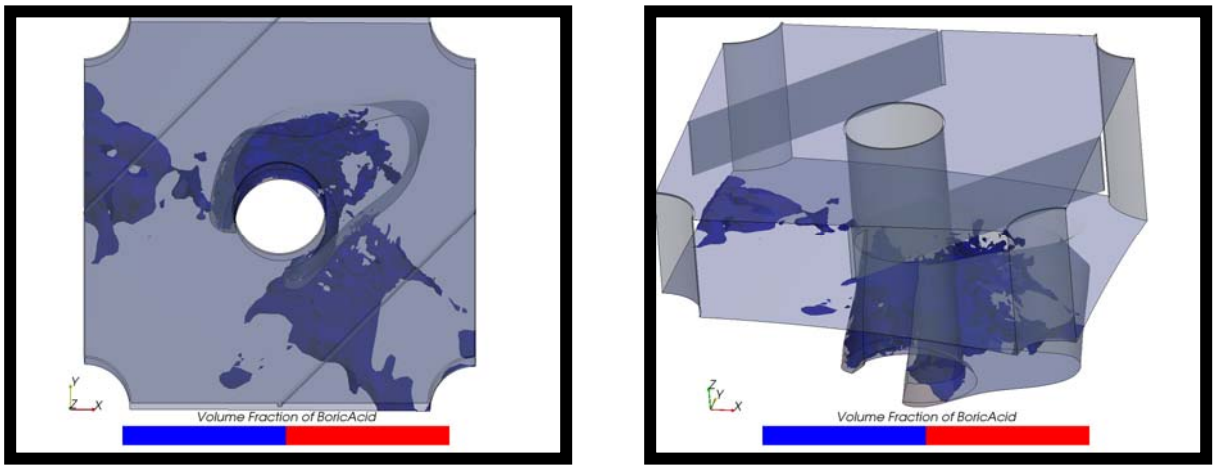

(c) Top View Time – 0.40 seconds Perspective View

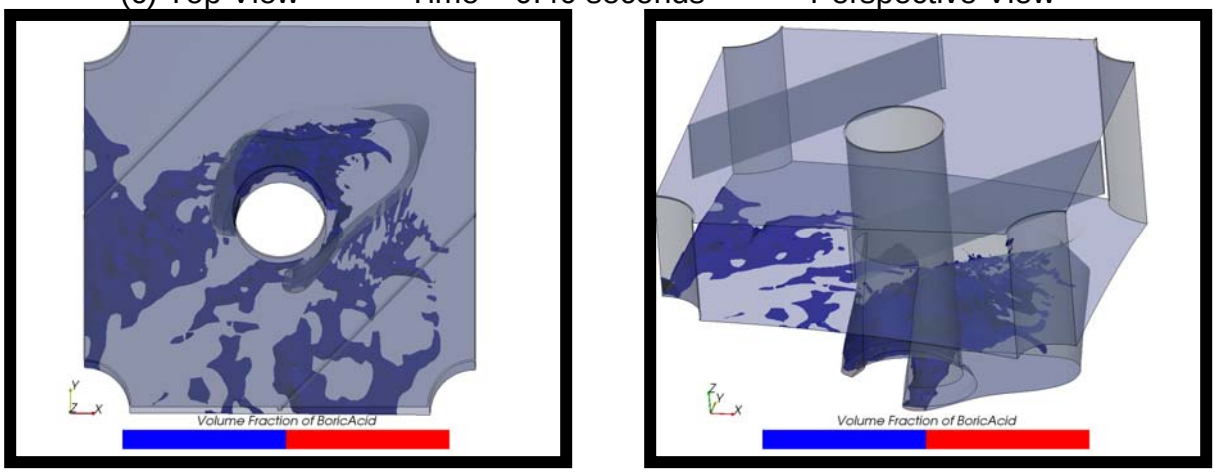

Figure 9.29 Transient analysis results for final wastage cavity filled with boric acid solution for time steps from 0.25 seconds to 0.40 seconds.

9.9 References

1. FENOC "Root Cause Analysis Report: Significant Degradation of the Reactor Pressure Vessel Head, CR 2002-0891, Dated 3-8-2002", Report Revision 1, August 27, 2002.

2. *Ibid*, Section 3.2.4, Page 25.

3. *Ibid*, Section 3.2.4, Page 25.

4. *Ibid*, Section 3.2.4, Page 26.

5. *Ibid*, Section 3.2.4, pages 26 through 28.

6. Dominion Engineering Inc., "Davis-Besse CRDM Leak Rates Using ANSYS Crack Opening Area (non-safety related)," Calculation Number: C-5509-00-6, Rev. 0, Undated.

7 "Root Cause Analysis Report: Significant Degradation of Reactor Pressure Vessel Head," Davis-Besse Report CR 2002-0891, Rev. 1, August 27, 2002, p. 108.

8 *Ibid*, page 20.

9 Dominion Engineering Inc., "Davis-Besse CRDM Leak Rates Using ANSYS Crack Opening Area (non-safety related)," Calculation Number: C-5509-00-6, Rev. 0, Undated, p. 3.

10 "Final Report: Examination of the Reactor Vessel (RV) Head Degradation at Davis-Besse," BWXT Services, Inc. Report 1140-025-02-24, June 2003, p. 42.

11 *Ibid*, page 160.

12 "Root Cause Analysis Report: Significant Degradation of Reactor Pressure Vessel Head," Davis-Besse Report CR 2002-0891, Rev. 1, August 27, 2002, p. 26

13 "Final Report: Examination of the Reactor Vessel (RV) Head Degradation at Davis-Besse," BWXT Services, Inc. Report 1140-025-02-24, June 2003, p. 51.

14 *Ibid*, page 82.

15 *Ibid*, page 58.

16 *Ibid*, page 59.

17 *Ibid*, page 82.